Distinct roles and actions of PDI family enzymes in catalysis of nascent-chain disulfide formation

Chihiro Hirayama[1], Kodai Machida[2#], Kentaro Noi[3#], Tadayoshi Murakawa[4], Masaki Okumura[1,5], Teru Ogura[6,7], Hiroaki Imataka[2], and Kenji Inaba[1*]

[1]Institute of Multidisciplinary Research for Advanced Materials, Tohoku University, Sendai, Miyagi 980-8577, Japan
[2]Graduate School of Engineering, University of Hyogo, Himeji, Hyogo 671-2280, Japan
[3]Institute for NanoScience Design, Osaka University, Toyonaka, Osaka 560-8531, Japan
[4]Graduate School of Life Science and Technology, Tokyo Institute of Technology, Yokohama, Kanagawa, 226-8503, Japan
[5]Frontier Research Institute for Interdisciplinary Sciences, Tohoku University, Sendai, Miyagi 980-8578, Japan
[6]Institute of Molecular Embryology and Genetics, Kumamoto University, Kumamoto, Kumamoto 860-0811, Japan
[7]Faculty of Life Sciences, Kumamoto University, Kumamoto 862-0973, Japan

[#]These authors contributed equally to this work

*Correspondence & Lead contact:
Kenji Inaba, Institute of Multidisciplinary Research for Advanced Materials, Tohoku University, Katahira 2-1-1, Aoba-ku, Sendai, Miyagi 980-8577, Japan
E-mail: kenji.inaba.a1@tohoku.ac.jp
Tel: +81-22-217-5604
Fax: +81-22-217-5605
ORCID: 0000-0001-8229-0467

Running title: Nascent-chain disulfide bond formation

Abstract

The mammalian endoplasmic reticulum (ER) harbors more than 20 members of the protein disulfide isomerase (PDI) family that act to maintain proteostasis. Herein, we developed an *in vitro* system for directly monitoring PDI- or ERp46-catalyzed disulfide bond formation in ribosome-associated nascent chains (RNC) of human serum albumin. The results indicated that ERp46 more efficiently introduced disulfide bonds into nascent chains with short segments exposed outside the ribosome exit site than PDI. Single-molecule analysis by high-speed atomic force microscopy further revealed that PDI binds nascent chains persistently, forming a stable face-to-face homodimer, whereas ERp46 binds for a shorter time in monomeric form, indicating their different mechanisms for substrate recognition and disulfide bond introduction. Similarly to ERp46, a PDI mutant with an occluded substrate-binding pocket displayed shorter-time RNC binding and higher efficiency in disulfide introduction than wild-type PDI. Altogether, ERp46 serves as a more potent disulfide introducer especially during the early stages of translation, whereas PDI can catalyze disulfide formation in RNC when longer nascent chains emerge out from ribosome.

Keywords

nascent chain, protein disulfide isomerase, ERp46, disulfide bond, co-translational folding, high-speed atomic force microscopy, ER proteostasis

Introduction

Over billions of years of evolution, living organisms have developed ingenious mechanisms to promote protein folding (Hartl *et al*, 2011). The oxidative network catalyzing protein disulfide bond formation in the endoplasmic reticulum (ER) is a prime example. While canonical protein disulfide isomerase (PDI) and ER oxidoreductin-1 (Ero1) were previously postulated to constitute a primary disulfide bond formation pathway (Araki & Inaba, 2012; Mezghrani *et al*, 2001; Tavender & Bulleid, 2010), more than 20 different PDI family enzymes and multiple PDI oxidases besides Ero1 have recently been identified in the mammalian ER, suggesting the development of highly diverse oxidative networks in higher eukaryotes (Nguyen *et al*, 2011; Schulman *et al*, 2010; Tavender *et al*, 2010). Each PDI family enzyme is likely to play a distinct role in catalyzing the oxidative folding of different substrates, concomitant with some functional redundancy, leading to the efficient production of a wide variety of secretory proteins with multiple disulfide bonds (Bulleid & Ellgaard, 2011; Okumura *et al*, 2015; Sato & Inaba, 2012).

Our previous *in vitro* studies using model substrates such as reduced and denatured bovine pancreatic trypsin inhibitor (BPTI) and ribonuclease A (RNase A) demonstrated that different PDI family enzymes participate in different stages of oxidative protein folding, resulting in the accelerated folding of native enzymes (Kojima *et al*, 2014; Sato *et al*, 2013). Multiple PDI family enzymes cooperate to synergistically increase the speed and fidelity of disulfide bond formation in substrate proteins. However, whether mechanistic insights gained by *in vitro* experiments using full-length substrates are applicable to real events of oxidative folding in the ER remains an important question. Indeed, some previous works demonstrated that newly synthesized

polypeptide chains undergo disulfide bond formation and isomerization co-translationally, presumably via catalysis by specific PDI family members (Kadokura *et al*, 2020; Molinari & Helenius, 1999; Robinson & Bulleid, 2020; Robinson *et al*, 2020; Robinson *et al*, 2017). Furthermore, nascent chains play important roles in their own quality control by modulating the translation speed to increase the yield of native folding; if a nascent chain fails to fold or complete translation, then the resultant aberrant ribosome-nascent chain complexes are degraded or destabilized (Buhr *et al*, 2016; Chadani *et al*, 2017; Matsuo *et al*, 2017). These observations suggest that understanding real events of oxidative protein folding in cells requires systematic analysis of how PDI family enzymes act on nascent polypeptide chains during synthesis by ribosomes.

To this end, we herein developed an experimental system for directly monitoring disulfide bond formation in ribosome-associated human serum albumin (HSA) nascent chains of different lengths from the N-terminus. The resultant ribosome-nascent chain complexes (RNCs) were reacted with two ubiquitously expressed PDI family members, ER-resident protein 46 (ERp46) and canonical PDI. These two enzymes were previously shown to have distinct roles in catalyzing oxidative protein folding: ERp46 engages in rapid but promiscuous disulfide bond introduction during the early stages of folding, while PDI serves as an effective proofreader of non-native disulfides during the later stages (Kojima *et al.*, 2014; Sato *et al.*, 2013). The subsequent maleimidyl polyethylene glycol (mal-PEG) modification of free cysteines and Bis-Tris (pH7.0) PAGE analysis enabled us to detect the oxidation status of the HSA nascent chains conjugated with transfer RNA (tRNA). Using high-speed atomic force microscopy (HS-AFM), we further visualized PDI and ERp46 acting on the RNCs

at the single-molecule level. Collectively, the results indicated that although both ERp46 and PDI could introduce a disulfide bond into the ribosome-associated HSA nascent chains, they demanded different lengths of the HSA segment exposed outside the ribosome exit site, and displayed different mechanisms of action against the RNC. The present systematic *in vitro* study using RNC containing different lengths of HSA nascent chains mimics co-translational disulfide bond formation in the ER, and the results provide a framework for understanding the mechanistic basis of oxidative nascent-chain folding catalyzed by PDI family enzymes.

Results

The efficiency of disulfide bond introduction into HSA nascent chains by PDI/ERp46

To investigate whether PDI family enzymes can introduce disulfide bonds into a substrate during translation, we first prepared RNCs *in vitro*. For this purpose, we made use of a cell-free protein translation system reconstituted with eukaryotic elongation factors 1 and 2, eukaryotic release factors 1 and 3 (eRF1 and eRF3), aminoacyl-tRNA synthetases, tRNAs, and ribosome subunits, developed previously by Imataka and colleagues (Machida *et al*, 2014). HSA was chosen as a model substrate for the following reasons. Firstly, the three-dimensional structure of HSA has been solved at high resolution (Sugio *et al*, 1999), providing information on the exact location of 17 disulfide bonds in its native structure. Secondly, native-state HSA contains an unpaired cysteine, Cys34, near the N-terminal region, which has potential to form a non-native disulfide bond with one of the subsequent cysteines, serving as a good indicator of whether a non-native disulfide is introduced by ERp46 or PDI during the early stage of

translation. Thirdly, overall conformation and kinetics of disulfide bond regeneration were characterized for reduced full-length HSA (Lee & Hirose, 1992), which is beneficial for discussing similarities and differences in post- and co-translational oxidative folding. Forth, no N-glycosylation sites are contained in the first 95 amino acids of HSA, implying that HSA nascent chains synthesized by the cell-free system are equivalent to those synthesized in the ER in regard to N-glycosylation. Finally, the involvement of PDI family enzymes in intracellular HSA folding has been demonstrated (Koritzinsky *et al*, 2013; Rutkevich *et al*, 2010; Rutkevich & Williams, 2012), ensuring the physiological relevance of the present study.

To stall the translation of HSA at specified sites, a uORF2 arrest sequence (Alderete *et al*, 1999) was inserted into appropriate sites of the expression plasmid (Fig 1A). We first prepared two versions of the RNC containing different lengths of HSA nascent chains: RNC 69-aa and RNC 82-aa. Since the ribosome exit tunnel accommodates a polypeptide chain of ~30 amino acid (aa) residues (Zhang *et al*, 2013), the N-terminal 57 residues of HSA (excluding the N-terminal 6-aa pro-sequence) are predicted to be exposed outside the ribosome exit tunnel in RNC 69-aa, including Cys34 and Cys53 (Fig 1A). In the RNC 82-aa construct, the N-terminal 70 residues of HSA, including Cys62 as well as Cys34/Cys53, are predicted to emerge from the ribosome (Fig 1A). Notably, Cys53 and Cys62 form a native disulfide bond, whereas Cys34 is unpaired in the native structure of HSA domain I.

When RNC 69-aa was employed as a substrate, neither PDI nor ERp46 could efficiently introduce a disulfide bond into the nascent chain (Fig 1C and 1D). However, both enzymes introduced a disulfide bond into RNC 82-aa with higher efficiency than into RNC 69-aa (Fig 1E and 1F), suggesting that the length of the exposed HSA

segment or the distance of a pair of cysteines from the ribosome exit site is critical for disulfide bond introduction by PDI and ERp46. For either construct, a faint band was seen between the bands of 'no SS' and '1 SS', and this band was even fainter without GSH/GSSG (the second lane from the left) and had a tendency to get stronger at late time points. Presumably, this band represents a species in which one of free cysteines is glutathionylated, and the species increased gradually in the course of the reaction.

Of note, ERp46 introduced a disulfide bond into RNC 82-aa at a much higher rate than PDI, indicating that ERp46 serves as a more competent disulfide bond introducer to RNCs than PDI (Fig 1F). The remarkable difference in disulfide bond introduction efficiency by these two enzymes seems unlikely to be explained simply by the different number of redox-active Trx-like domains in PDI (two) and ERp46 (three) (Fig 1B). Also, the redox states in the presence of 1 mM GSH and 0.2 mM GSSG are similar between these two enzymes (Fig EV1A and EV1B), suggesting their comparable redox potentials. Thus, the different ability of ERp46 and PDI to introduce a disulfide into 82-aa is likely caused by other factors such as different structural features and different mechanism of substrate recognition, as discussed below.

Next, to identify which cysteine pair forms a disulfide bond in RNC 82-aa, we constructed three cysteine mutants in which either Cys34, Cys53, or Cys62 was mutated to alanine (Fig 2A). The assays using the mutants showed that whereas PDI was unable to introduce a disulfide bond into RNC 82-aa C34A and C53A (Fig 2B, top and middle), the enzyme introduced a Cys34-Cys53 non-native disulfide bond into RNC 82-aa C62A (Fig 2B, bottom), at almost the same rate as the generation of the '1 SS' species in 82-aa (Fig 1E and 1F). PDI could not introduce a Cys53-Cys62 native disulfide bond, presumably because this cysteine pair is located too close to the ribosome exit site (see

174 also Fig 3B and 3C). Conversely, the slow but possible formation of a Cys34-Cys53
175 non-native disulfide in 82 aa by PDI suggests that the distance between a cysteine pair
176 of interest and the ribosome exit site is key to allowing the enzyme to catalyze disulfide
177 bond introduction into RNCs. Considering the different locations of the Cys34-Cys53
178 and Cys53-Cys62 pairs on RNC 82-aa, a distance of ~18 residues from the ribosome
179 exit site appears to be necessary for the PDI-catalyzed reaction (see also the
180 Discussion).

181 In contrast to PDI, ERp46 could introduce a native disulfide bond into RNC
182 82-aa C34A (Fig 2C, top). Like PDI, ERp46 also introduced a non-native disulfide bond
183 between Cys34 and Cys53 into RNC 82-aa C62A, but its efficiency was lower than that
184 of a Cys53-Cys62 native disulfide (Fig 2C, bottom). No disulfide bond was formed
185 between Cys34 and Cys62 by either ERp46 or PDI (Fig 2C, middle), presumably due to
186 the considerable spatial separation of these two cysteines. Based on these results, we
187 concluded that for efficient disulfide bond introduction into RNCs, ERp46 requires an
188 intermediary polypeptide segment with a shorter distance between a cysteine pair of
189 interest and the ribosome exit site than PDI. We here note that ERp46-catalyzed
190 generation of the '1 SS' species was faster in 82-aa than in 82-aa C34A (Fig 1F and 2C).
191 This observation may suggest the occurrence of Cys34-mediated disulfide bond
192 formation in 82-aa, namely, the formation of a Cys34-Cys53 non-native disulfide and,
193 possibly, its rapid isomerization to a Cys53-Cys62 native disulfide.

194

195 **Accessibility of PDI/ERp46 to cysteines on the ribosome-HSA nascent chain**
196 **complex**

197 To examine the accessibility of PDI and ERp46 to Cys residues on RNC 82-aa, we

198 constructed three RNC 82-aa mono-Cys mutants in which either Cys34, Cys53, or
199 Cys62 on the HSA nascent chain was retained, and investigated whether a mixed
200 disulfide could be formed between the RNC 82-aa mutant and a trapping mutant of PDI
201 or ERp46 in which all CXXC redox-active sites were mutated to CXXA. Both PDI and
202 ERp46 formed a mixed disulfide bond with Cys34 and Cys53 on RNC 82-aa with high
203 probability, but covalent linkages to Cys62 were marginal (Fig 2D and 2E). The results
204 suggest that the redox-active sites of PDI and ERp46 could gain access to Cys34 and
205 Cys53, but to a much lesser extent, to Cys62, probably due to steric collision with the
206 ribosome. Nevertheless, ERp46 efficiently introduced a native disulfide bond between
207 Cys53 and Cys62 (Fig 2C, top), presumably because ERp46 first attacked Cys53 on the
208 HSA nascent chain, and the resultant mixed disulfide was subjected to nucleophilic
209 attack by Cys62 (Fig 2F, right). By contrast, the mixed disulfide between PDI and
210 Cys53 on the HSA nascent chain seems unlikely to be attacked by Cys62, probably due
211 to steric collision between PDI and the ribosome (Fig 2F, left). In line with this idea,
212 PDI adopts a U-like overall conformation with restricted movements of four thioredoxin
213 (Trx)-like domains (Tian *et al*, 2006; Wang *et al*, 2012), whereas ERp46 forms a highly
214 flexible V-shape conformation composed of three Trx-like domains and two long (~20
215 aa) interdomain linkers (Kojima *et al.*, 2014).
216
217 **Correlations between cysteine accessibility and the efficiency of disulfide bond**
218 **introduction by PDI/ERp46**
219 Based on the results presented above, we believe that the distance between cysteines of
220 interest and the ribosome exit site is critical for efficient disulfide introduction by PDI
221 and ERp46. To test this hypothesis, we increased the distance of the Cys53-Cys62 pair

222 from the ribosome exit site by inserting an extended polypeptide segment composed of
223 $[SG]_5$ or $[SG]_{10}$ repeat immediately after Cys62 on RNC 82-aa C34A (Fig 3A), and
224 investigated the effects of the insertions on the efficiency of disulfide bond formation.
225 While PDI was unable to introduce a Cys53-Cys62 native disulfide into RNC 82-aa
226 C34A (Fig 2B, top), insertion of a $[SG]_5$ repeat allowed this reaction, and nearly 70% of
227 82-aa C34A was disulfide-bonded within a reaction time of 360 s (Fig 3B, upper and
228 3C). The insertion of a longer repeat $[SG]_{10}$ further promoted disulfide bond formation
229 (Fig 3B, lower and 3C).

230 A similar enhancement following [SG] repeat insertion was observed for
231 ERp46-catalyzed reactions. However, ERp46 exhibited a striking difference from PDI:
232 insertion of a $[SG]_5$ repeat was long enough to introduce a Cys53-Cys62 native disulfide
233 into RNC 82-aa C34A within 15 s, and insertion of a $[SG]_{10}$ repeat gave only a small
234 additional enhancement (Fig 3D and 3E). Thus, the presence of a disordered or
235 extended segment of ~18 aa (Asp63–Phe70 + $[SG]_5$ repeat) between a cysteine pair of
236 interest and the ribosome exit site was necessary and sufficient for ERp46 to generate a
237 Cys53-Cys62 disulfide rapidly, whereas PDI required a longer segment of ~28 aa
238 (Asp63–Phe70 + $[SG]_{10}$ repeat) in this intermediary region for efficient introduction of
239 a Cys53-Cys62 disulfide. Thus, ERp46 seems to be more capable of introducing a
240 disulfide bond near the ribosome exit site than PDI. In other words, ERp46 likely has
241 the higher potential to introduce a disulfide bond into the HSA nascent chain during the
242 earlier stages of translation than PDI.

243 To verify that Cys53-Cys62 disulfide formation facilitated by $[SG]_{10}$ repeat
244 insertion was ascribed to higher accessibility of PDI/ERp46 to Cys62, we again
245 investigated mixed disulfide bond formation between trapping mutants of PDI/ERp46

and each cysteine on RNC 82-aa following $[SG]_{10}$ repeat insertion. Both PDI and ERp46 formed a mixed disulfide with all cysteines including Cys62 (Fig 3F and 3G), indicating that there is a correlation between the accessibility of PDI/ERp46 to a target pair of cysteines and the efficiency of disulfide bond introduction by the enzymes.

Disulfide bond introduction into a longer HSA nascent chain by PDI/ERp46

In addition to the [SG]-repeat insertion, we examined the effect of natural HSA sequence extension on PDI- or ERp46-mediated disulfide formation. For this purpose, we prepared RNC 95-aa in which the N-terminal 83 amino acids of HSA (excluding the N-terminal 6-aa pro-sequence), including Cys34, Cys53, Cys62, and Cys75, are predicted to emerge from ribosome (Fig 4A). With this construct, however, we had a technical problem with detection of the reduced species, because mal-PEG modification of four cysteines greatly diminished the gel-to-membrane transfer efficiency. We overcame this problem by using photo-cleavable mal-PEG (PEG-PCMal) and irradiating UV light to the SDS gel after the gel electrophoresis and before the membrane transfer.

Consequently, we observed both PDI and ERp46 introduced a disulfide bond into 95-aa (Fig 4B), but the efficiency was slower than that into 82-aa (Fig 1E and 1F), although a longer polypeptide chain is exposed outside the ribosome exit site in RNC 95-aa. Thus, the effect of natural sequence extension was opposite to that of [SG]-repeat insertion. Formation of some higher-order structure or exposure of another cysteine may somehow prevent PDI and ERp46 from introducing a disulfide bond into RNC 95-aa. Thus, a longer polypeptide chain exposed outside ribosome does not always lead to a higher disulfide formation rate. Rather, it is suggested that PDI and ERp46 can

introduce a disulfide bond into a nascent chain with higher efficiency when the necessary and minimum length emerges out.

Given that four cysteines are exposed outside the ribosome in RNC 95-aa, we next investigated whether PDI and ERp46 can catalyze nascent-chain disulfide formation additionally or synergistically. The mixture of PDI and ERp46 generated a '1 SS' species, but not a '2 SS' species, like PDI or ERp46 alone (Fig 4B and 4C). Notably, the presence of PDI inhibited ERp46-mediated disulfide formation, possibly due to its competition with ERp46 for binding to RNC 95-aa. Thus, neither additional nor synergistic effect was observed (Fig 4B and 4C). In this regard, our previous observation for the synergistic cooperation of PDI and ERp46 in RNase A oxidative folding (Sato *et al.*, 2013) was not true for the ribosome-associated HSA nascent chain.

Single-molecule analysis of ERp46 by high-speed atomic force microscopy

To explore the mechanisms by which PDI and ERp46 recognize and act on RNCs at the molecular level, we employed HS-AFM (Kodera *et al*, 2010; Noi *et al*, 2013; Okumura *et al*, 2019; Uchihashi *et al*, 2018). While our previous HS-AFM analysis revealed that PDI molecules form homodimers in the presence of unfolded substrates (Okumura *et al.*, 2019), the structure and dynamics of ERp46 have not been analyzed using this experimental approach. Therefore, we first observed ERp46 molecules alone by immobilizing the N-terminal His-tag on a Co^{2+}-coated mica surface. AFM images revealed various overall shapes of ERp46 (Fig 5A), and some particle images clearly demonstrated the presence of three thioredoxin (Trx)-like domains in ERp46 (Fig 5A, left). To assess the overall structures of ERp46, we calculated the circularity of each molecule and performed statistical analysis (Uchihashi *et al.*, 2018). Circularity is a

measure of how circular the outline of an observed molecule is, defined by the equation $4\pi S/L^2$, where L and S are the contour length of the outline and the area surrounded by the outline, respectively. Thus, a circularity of 1.0 indicates a perfect circle, and values <1 indicate a more extended conformation.

Statistical analysis based on circularity classified randomly chosen ERp46 particles into two major groups: opened V-shape and round/compact O-shape (Fig 5A). Histograms with Gaussian fitting curves indicated that ~80% of ERp46 molecules adopted V-shape conformations while ~20% adopted O-shape conformations (Fig 5B). There was no large difference in height between these two conformations, suggesting that the three Trx-like domains of ERp46 are arranged within the same plane in either conformation. Successive AFM images acquired every 100 ms revealed that ERp46 adopted an open V-shape conformation during nearly 75% of the observation time, while the protein also adopted an O-shape conformation occasionally (Fig 5C, 5D, 5E and Movie EV1). The histogram calculated from the time-course snapshots was similar to that calculated from images of 200 molecules at a certain timepoint (Fig 5B and 5E). Importantly, structural insights gained by HS-AFM analysis are in good agreement with those from small-angle X-ray scattering (SAXS) analysis: both analyses consistently indicate the coexistence of a major population of molecules with an open V-shape and a minor population with a compact O-shape (Kojima *et al.*, 2014).

Single-molecule analysis of PDI/ERp46 acting on 82-aa RNC by HS-AFM

PDI and ERp46 are predicted to bind RNCs transiently during disulfide bond introduction, but transient interactions would make it harder to observe and analyze the mode of PDI/ERp46 binding to RNCs. More practically, at least 5 mins are required to

prepare for starting HS-AFM measurements after adding PDI or ERp46 to RNCs immobilized onto a mica surface. If we employed RNCs containing natural HSA sequences, PDI or ERp46 would complete nascent-chain disulfide formation during this setup time. We therefore constructed HSA 82-aa RNC with Cys34, Cys53, and Cys62 mutated to Ala (hereafter referred to as 82-aa CA RNC), with the intension of trapping RNC molecules bound to PDI/ERp46. After testing several RNC immobilization methods, we chose to immobilize RNC on a Ni^{2+}-coated mica surface. As a result, most RNC molecules were observed to lie sideways on the mica surface, while nascent chains were difficult to visualize, probably due to their flexible and extended structural nature (Fig 6A).

When oxidized PDI or ERp46 were added to onto the RNC-immobilized mica surface, PDI/ERp46-like particles were observed in the peripheral region of ribosomes. When no-chain RNC (NC-RNC), comprising only the N-terminal FLAG tag and the subsequent uORF2 but no segment from HSA, was immobilized on the mica surface, far fewer particles were observed near RNCs (within 25 Å from the outline of ribosomes) by HS-AFM despite the presence of PDI/ERp46 (Fig EV2A and EV2B). These results confirm that we successfully observed PDI/ERp46 molecules acting on HSA nascent chains associated with ribosomes.

Notably, the HS-AFM analysis revealed that PDI bound RNCs in both monomeric and dimeric forms at an approximate ratio of 7:3 (Fig 6B), as reported previously for reduced and denatured BPTI and RNase A as substrates (Okumura *et al.*, 2019). Thus, PDI likely recognizes HSA nascent chains in a similar manner to full-length substrates. Statistical analysis of RNC binding rates revealed that whereas most monomeric PDI molecules (52/55 molecules) bound RNC for 10 s or shorter (Fig

6D, Fig EV3A and Movie EV2), most homodimeric PDI molecules (17/19 molecules) bound RNC for 60 s or longer (Fig 6D, Fig EV3B and Movie EV3). By contrast, ERp46 molecules in the periphery of RNCs were only present in monomeric form (Fig 6C). Importantly, nearly 20% (12/59 molecules) of ERp46 molecules bound RNC for 10 to 20 s (Fig 6D, Fig EV3C and Movie EV4), while a smaller portion (8/59 molecules) bound RNC for ~60 s (Fig 6D). It is also notable that significant portion of PDI and ERp46 molecules bound ribosomes for <5 s. This may indicate that PDI/ERp46 binds or approaches RNCs only transiently possibly via diffusion, without tight interactions.

The histogram of the distance between the edge of ribosomes and the center of ribosome-neighboring PDI/ERp46 molecules indicated that both PDI and ERp46 bound RNCs at positions ~16 nm distant from ribosomes with a single-Gaussian distribution with a half width of ~11 nm (Fig 6E), suggesting that both enzymes recognize similar sites of the HSA nascent chain. Given that the distance between adjacent amino acids is approximately 3.5 Å along an extended strand, Cys34, Cys53, and Cys62 are calculated to be 130 Å, 63 Å, and 35 Å distant from the ribosome exit site, respectively. The distributions of PDI and ERp46 molecules bound to RNC 82-aa seem consistent with their accessibility to Cys34 and Cys53, but not to Cys62, as revealed by their mixed disulfide formation with RNC 82-aa (Fig 2D and E).

Role of the PDI hydrophobic pocket in oxidation of the HSA nascent chain

It is widely known that the PDI **b'** domain contains a hydrophobic pocket that acts as a primary substrate-binding site (Klappa *et al*, 1998). To examine the involvement of the hydrophobic pocket in PDI-catalyzed disulfide bond formation in the HSA nascent chain, we mutated I289, one of the central residues that constitute the hydrophobic

366 pocket, to Ala, and compared the efficiency of disulfide bond introduction into RNC
367 82-aa between wild-type (WT) and mutant I289A proteins. In this mutant, the x-linker
368 flanked by **b'** and **a'** domains tightly binds the hydrophobic pocket, unlike in WT,
369 thereby preventing PDI from tightly binding an unfolded substrate (Bekendam *et al*,
370 2016; Nguyen *et al*, 2008). ERp57, another primary member of the PDI family, has a
371 U-shape domain arrangement similar to PDI, but does not contain the hydrophobic
372 pocket in the **b'** domain. For comparison, we also monitored ERp57-catalyzed disulfide
373 introduction into RNC 82-aa.

374 Despite the occlusion or lack of the hydrophobic substrate-binding pocket, both
375 PDI I289A and ERp57 were found to introduce a disulfide bond into RNC 82-aa at a
376 higher rate than PDI WT (Fig 7A and B). This result suggests that the hydrophobic
377 pocket is involved in binding the HSA nascent chain, but this binding appears to rather
378 slow down disulfide introduction into a nascent chain.

379 To further explore the mechanism by which PDI I289A introduced a disulfide
380 bond at a faster rate than PDI WT, we analyzed its binding to RNC using HS-AFM. The
381 analysis revealed that, while nearly one-third of PDI I289A molecules formed dimers in
382 the presence of RNC 82-aa like PDI WT, the mutant dimers bound RNC for a shorter
383 time than the WT dimers (Fig 7C and Movie EV6). Thus, the RNC-binding time of PDI
384 I289A showed similar distribution to that of ERp46 (Fig 7D and Movies EV5 and EV6),
385 which seems consistent with the higher disulfide introduction efficiency of PDI I289A
386 than that of PDI WT. PDI I289A also bound RNCs at positions ~16 nm distant from
387 ribosome with a single-Gaussian distribution (Fig 7E), suggesting that PDI I289A
388 recognizes similar sites of the HSA nascent chain as PDI and ERp46.
389

Discussion

A number of studies have recently investigated co-translational oxidative folding in the ER (Kadokura *et al.*, 2020; Robinson *et al.*, 2020; Robinson *et al.*, 2017). The present study showed that while both PDI and ERp46 can introduce a disulfide bond into a nascent chain co-translationally, ERp46 catalyzes this reaction more efficiently than PDI and requires a shorter nascent chain segment exposed outside the ribosome exit. Thus, ERp46 appears to be capable of introducing a disulfide bond into a nascent chain during the earlier stages of translation than PDI. The efficient introduction of a Cys53-Cys62 native disulfide on RNC 82-aa by ERp46 (Fig 2) suggests that a separation of ~8 aa residues between a C-terminal cysteine on a nascent chain and the ribosome exit site (i.e., residues 63-70) is sufficient for ERp46 to catalyze this reaction (Fig 8). When a nascent chain was elongated by the insertion of [SG]-repeat sequences, PDI could also introduce the native disulfide bond into RNCs to some extent (Fig 3B and 3C). Thus, PDI appears to act on a nascent chain to introduce a disulfide bond when the distance between a C-terminal cysteine on a nascent chain and the ribosome exit site reaches ~18 aa residues (i.e., residues 63-70 + $[SG]_5$ repeat; Fig 8).

Disulfide bond formation in partially ER-exposed nascent chains was indeed observed with the ADAM10 disintegrin domain, which has a dense disulfide bonding pattern and little defined structure (Robinson *et al.*, 2020). Thus, disulfide bond formation seems to be allowed before the higher order structure is defined in a nascent chain. This could be the case with a Cys34-Cys53 nonnative disulfide and a Cys53-Cys62 native disulfide on RNC 82-aa, since the N-terminal 82-residue HSA fragment alone is unlikely to fold to a globular native-like structure though the fragment of residue 35 to 56 is predicted to form an α-helix according to the HSA native structure.

In contrast, some proteins including β2-microglobulin (β2M) and prolactin are shown to form disulfide bonds only after a folding domain is fully exposed to the ER or a polypeptide chain is released from ribosome, suggesting their folding-driven disulfide bond formation. Notably, PDI binds β2M when the N-terminal ~80 residues of β2M are exposed to the ER, and completes disulfide bond introduction at the even later stages of translation (Robinson *et al.*, 2017). Thus, PDI has been demonstrated to engage in disulfide bond formation during late stages of translation or after translation in the ER.

Regarding mechanistic insight, the present HS-AFM analysis visualized PDI and ERp46 acting on nascent chains at the single-molecule level. We found that PDI forms a face-to-face homodimer that binds a nascent chain, as is the case with reduced and denatured full-length substrates (Okumura *et al.*, 2019). On the other hand, ERp46 maintains a monomeric form while binding a nascent chain. Interestingly, the PDI dimer binds a nascent chain much more persistently than the PDI monomer and ERp46, suggesting that the PDI dimer holds a nascent chain tightly inside its central hydrophobic cavity. In agreement with this observation, a hydrophobic-pocket mutant (I289A) of PDI bound a nascent chain for shorter time and introduced a disulfide bond into a nascent chain more rapidly than the WT enzyme, as was the case with ERp46. In this context, PDI competed with ERp46 for acting on RNC 95-aa, and thereby inhibited ERp46-mediated disulfide introduction (Fig 4 and Fig 8). Thus, PDI family enzymes do not always work synergistically to accelerate oxidative protein folding, but may possibly inhibit each other during co-translational disulfide bond formation.

How the ER membrane translocon channel is involved in co-translational oxidative folding catalyzed by PDI family enzymes remains an important question. It is possible that PDI and ERp46 form a supramolecular complex with ribosomes and the

Sec61 translocon channel via a nascent chain. Indeed, PDI was previously identified as a luminal protein that was in close contact with translocating nascent chains (Klappa *et al*, 1995). Additionally, the oligosaccharyltransferase complex (Harada *et al*, 2009) and an ER chaperone calnexin (Farmery *et al*, 2000) have been reported to interact with the ribosome-associated Sec61 channel to catalyze N-glycosylation and folding of nascent chains in the ER, respectively. In this regard, it will be interesting to examine the close co-localization of PDI/ERp46 with the Sec61 channel in the presence or absence of nascent chains in transit into the ER lumen by super-resolution microscopy or other tools. Systematic studies with a wider range of substrates of different lengths from the ribosome exit site and different numbers of cysteine pairs, and with other PDI family members potentially having different functional roles, will provide further mechanistic and physiological insights into co-translational oxidative folding and protein quality control in the ER.

Materials & Methods

Construction of HSA plasmids

DNA fragments encoding specific regions (69-aa, N-terminal pro-sequence 6-aa + the subsequent 63-aa; 82-aa, N-terminal pro-sequence 6-aa + the subsequent 76-aa; 95-aa, N-terminal pro-sequence 6-aa + the subsequent 89-aa) of HSA were amplified by PCR with appropriate primers and inserted into the pUC-T7-HCV-FLAG-2A-uORF expression plasmid, as described in Machida et al. (2014). The amplified fragments were replaced with the 2A region to generate pUC-T7-HCV-FLAG-HSA (69-aa or 82-aa)-uORF2. RNC 82-aa C34A/C53A/C62A and mono-Cys mutants were constructed using the QuikChange method with appropriate primers (Table 1). RNC 82-aa C34A

462 with $[SG]_5$ or $[SG]_{10}$ repeats were constructed by the Prime STAR MAX (Takara Bio
463 Inc., Japan) method using appropriate primers (Table 1).
464
465 ***Expression and purification of PDI and ERp46***
466 Overexpression and purification of human PDI and ERp46, and their mutants, were
467 performed as described previously (Kojima *et al.*, 2014; Sato *et al.*, 2013). An ERp46
468 trapping mutant with a CXXA sequence in all Trx-like domains was constructed by the
469 QuikChange method using appropriate sets of primers.
470
471 ***Preparation of RNCs using a translation system reconstituted with human factors***
472 A cell-free translation system was reconstituted with eEF1 (50 μM), eEF2 (1 μM),
473 eRF1/3 (0.5 μM), aminoacyl-tRNA synthetases (0.15 μg/μl), tRNAs (1 μg/μl), 40S
474 ribosomal subunit (0.5 μM), 60S ribosomal subunit (0.5 μM), PPA1 (0.0125 μM),
475 amino acids mixture (0.1 mM) and T7 RNA polymerase (0.015 μg/μl) (Machida *et al.*,
476 2014). We added 1.0 μL template plasmid (0.5 mg/mL) into 19 μL of this cell-free
477 system, and the mixture was incubated for at least 3–4.5 h at 32°C. After HKMS buffer
478 (comprising 25 mM HEPES-KOH (pH 7.0), 150 mM KCl, 5 mM $Mg(OAc)_2$, and 1.0 M
479 sucrose) was added, samples were ultra-centrifuged at 100,000 g overnight at 4 °C to
480 recover the RNC as a pellet. After removing the supernatant, pellets were resuspended
481 in HKM buffer comprising 25 mM HEPES-KOH (pH 7.0), 150 mM KCl, and 5 mM
482 $Mg(OAc)_2$.
483
484 ***Monitoring PDI- and ERp46-mediated disulfide bond introduction into RNCs***

The RNC suspension prepared as described above was mixed with PDI or ERp46 (0.1 μM each) and glutathione/oxidized glutathione (GSH/GSSG; 1.0 mM:0.2 mM; NACALAI TESQUE, INC., Japan). Aliquots were collected after incubation at 30°C for the indicated times, and reactions were quenched with mal-PEG 5K (2 mM; NOF CORPORATION, Japan) for RNC 69-aa and RNC 82-aa. After cysteine alkylation at room temperature for 20 min, samples were separated by 12% Bis-Tris (pH7.0) PAGE (Thermo Fisher Scientific K.K., Japan) in the presence of the reducing reagent β-mercaptoethanol (β-ME; 10% v/v; NACALAI TESQUE, INC., Japan). After transferring onto a polyvinylidene fluoride (PVDF) membrane (Merck KGaA, Darmstadt, Germany), bands on the membrane were visualized using Chemi-Lumi One Ultra (NACALAI TESQUE, INC., Japan) and a ChemiDocTM Imaging System (Bio-Rad Laboratories, Inc., CA, USA). Signal intensity was quantified using ImageLab software (Bio-Rad Laboratories, Inc., CA, USA).

For RNC 95-aa, reactions were quenched with PEG-PCMal (Dojindo, Japan). After cysteine alkylation at room temperature for 20 min, samples were separated by 10% Bis-Tris (pH7.0) PAGE (Thermo Fisher Scientific K.K., Japan) in the presence of the reducing reagent β-ME (10% v/v;). After gel electrophoresis, the gel was subjected to UV irradiation (302 nm, 8 W) for 30 min. The subsequent procedures were the same as described above.

Monitoring intermolecular disulfide bond linkage between PDI/ERp46 and ribosome-HSA nascent chain complexes

To detect the intermolecular disulfide bond linkage between PDI/ERp46 and the ribosome-HSA nascent chain complex, we employed RNC 82-aa mono-Cys mutants

retaining one of Cys34, Cys53, or Cys62. The RNC suspension prepared as described above was mixed with a PDI or ERp46 trapping mutant (1 μM each) and diamide (100 μM). Aliquots were collected after incubation at 30°C for 10 min, and reactions were quenched with N-ethylmaleimide (2 mM; NACALAI TESQUE, INC., Japan). Samples were analyzed by Nu-PAGE and western blotting as described above.

High-speed atomic force microscopy imaging

The structural dynamics of PDI and ERp46 were probed using a high-speed AFM instrument developed by Toshio Ando's group (Kanazawa University). Data acquisition for ERp46 was performed as described previously (Okumura *et al.*, 2019). Briefly, His_6-tagged ERp46 was immobilized on a Co^{2+}-coated mica surface through the N-terminal His-tag. To this end, a droplet (10 μL) containing 1 nM ERp46 was loaded onto the mica surface. After a 3 min incubation, the surface was washed with TRIS buffer (50 mM TRIS-HCl pH7.4, 300 mM NaCl). Single-molecule imaging was performed in tapping mode (spring constant, ~0.1 N/m; resonant frequency, 0.8–1 MHz; quality factor in water, ~2) and analyzed using Kodec4.4.7.39 software developed by Toshio Ando's group (Kanazawa University). AFM observations were made in fixed imaging areas (400 × 400 $Å^2$) at a scan rate of 0.1 s/frame. Each molecule was observed separately on a single frame with the highest pixel setting (60 × 60 pixels). Cantilevers (Olympus, Tokyo, Japan) were 6–7 μm long, 2 μm wide, and 90 nm thick. For AFM imaging, the free oscillation amplitude was set to ~1 nm, and the set-point amplitude was around 80% of the free oscillation amplitude. The estimated tapping force was <30 pN. A low-pass filter was used to remove noise from acquired images. The area of a single ERp46 molecule in each frame was calculated using LabView 2013 (National

Instruments, Austin, TX, USA) with custom-made programs.

To observe the binding of PDI/ERp46 to RNCs by HS-AFM, RNCs were immobilized on a Ni^{2+}-coated mica surface via electrostatic interactions. To this end, a droplet (10 μL) containing RNCs was loaded onto the mica surface. After a 10 min incubation, the surface was washed with HSA buffer comprising 25 mM HEPES-KOH pH 7.0, 150 mM KCl, and 5 mM $Mg(OAc)_2$. PDI/ERp46 lacking the N-terminal His_6-tag was added to the RNC-immobilized mica surface at a final concentration of 1 nM. Measurements were performed under the same conditions described above.

Acknowledgments

This work was supported by Grants-in-Aid for Scientific Research from MEXT to KI (26116005 and 18H03978), the NAGASE Science Technology Foundation (K.I.) and the MITSUBISHI Foundation (K.I.). This work was also supported by Grant-in-Aid for JSPS Fellows (Grant Number 20J11932 to C.H.) and a Grant-in-Aid of Tohoku University, Division for Interdisciplinary Advanced Research and Education (to C.H.).

Author contributions

C.H. and T.M. developed an experimental system for directly monitoring co-translational disulfide bond formation. K.M. and H.I. developed and prepared cell-free protein translation system reconstituted with human factors. C.H. prepared various plasmids. C.H. and M.O. purified PDI and ERp46, and their mutants. C.H. and K.N. performed HS-AFM measurements and analyses. C.H., K.N., M.O. and T.O. discussed the results of HS-AFM. K.I. supervised the work. C.H. and K.N. prepared the Figures. C.H. and K.I. wrote the manuscript. All of the authors discussed the results and

approved the manuscript.

Conflict of interests

We declare that there are no competing interests related to this work.

References

Alderete JP, Jarrahian S, Geballe AP (1999) Translational effects of mutations and polymorphisms in a repressive upstream open reading frame of the human cytomegalovirus UL4 gene. *J Virol* 73: 8330-8337

Araki K, Inaba K (2012) Structure, mechanism, and evolution of Ero1 family enzymes. *Antioxidants & redox signaling* 16: 790-799

Bekendam RH, Bendapudi PK, Lin L, Nag PP, Pu J, Kennedy DR, Feldenzer A, Chiu J, Cook KM, Furie B *et al* (2016) A substrate-driven allosteric switch that enhances PDI catalytic activity. *Nature communications* 7: 12579

Buhr F, Jha S, Thommen M, Mittelstaet J, Kutz F, Schwalbe H, Rodnina MV, Komar AA (2016) Synonymous Codons Direct Cotranslational Folding toward Different Protein Conformations. *Molecular cell* 61: 341-351

Bulleid NJ, Ellgaard L (2011) Multiple ways to make disulfides. *Trends in biochemical sciences* 36: 485-492

Chadani Y, Niwa T, Izumi T, Sugata N, Nagao A, Suzuki T, Chiba S, Ito K, Taguchi H (2017) Intrinsic Ribosome Destabilization Underlies Translation and Provides an Organism with a Strategy of Environmental Sensing. *Molecular cell* 68: 528-539.e525

Farmery MR, Allen S, Allen AJ, Bulleid NJ (2000) The role of ERp57 in disulfide bond formation during the assembly of major histocompatibility complex class I in a synchronized semipermeabilized cell translation system. *The Journal of biological chemistry* 275: 14933-14938

Harada Y, Li H, Li H, Lennarz WJ (2009) Oligosaccharyltransferase directly binds to ribosome at a location near the translocon-binding site. *Proceedings of the National Academy of Sciences of the United States of America* 106: 6945-6949

Hartl FU, Bracher A, Hayer-Hartl M (2011) Molecular chaperones in protein folding and proteostasis. *Nature* 475: 324-332

Kadokura H, Dazai Y, Fukuda Y, Hirai N, Nakamura O, Inaba K (2020) Observing the nonvectorial yet cotranslational folding of a multidomain protein, LDL receptor, in the ER of mammalian cells. *Proceedings of the National Academy of Sciences of the United States of America* 117: 16401-16408

Klappa P, Freedman RB, Zimmermann R (1995) Protein disulphide isomerase and a lumenal cyclophilin-type peptidyl prolyl cis-trans isomerase are in transient contact with secretory proteins during late stages of translocation. *Eur J Biochem* 232: 755-764

Klappa P, Ruddock LW, Darby NJ, Freedman RB (1998) The b' domain provides the principal peptide-binding site of protein disulfide isomerase but all domains contribute to binding of misfolded proteins. *The EMBO journal* 17: 927-935

Kodera N, Yamamoto D, Ishikawa R, Ando T (2010) Video imaging of walking myosin V by high-speed atomic force microscopy. *Nature* 468: 72-76

Kojima R, Okumura M, Masui S, Kanemura S, Inoue M, Saiki M, Yamaguchi H, Hikima T, Suzuki M, Akiyama S *et al* (2014) Radically different thioredoxin domain arrangement of ERp46, an efficient disulfide bond introducer of the mammalian PDI family. *Structure (London, England : 1993)* 22: 431-443

Koritzinsky M, Levitin F, van den Beucken T, Rumantir RA, Harding NJ, Chu KC, Boutros PC, Braakman I, Wouters BG (2013) Two phases of disulfide bond formation have differing requirements for oxygen. *The Journal of cell biology* 203: 615-627

Lee JY, Hirose M (1992) Partially folded state of the disulfide-reduced form of human serum albumin as an intermediate for reversible denaturation. *The Journal of biological chemistry* 267: 14753-14758

Machida K, Mikami S, Masutani M, Mishima K, Kobayashi T, Imataka H (2014) A translation system reconstituted with human factors proves that processing of encephalomyocarditis virus proteins 2A and 2B occurs in the elongation phase of translation without eukaryotic release factors. *The Journal of biological chemistry* 289: 31960-31971

Matsuo Y, Ikeuchi K, Saeki Y, Iwasaki S, Schmidt C, Udagawa T, Sato F, Tsuchiya H, Becker T, Tanaka K *et al* (2017) Ubiquitination of stalled ribosome triggers ribosome-associated quality control. *Nature communications* 8: 159

Mezghrani A, Fassio A, Benham A, Simmen T, Braakman I, Sitia R (2001) Manipulation of oxidative protein folding and PDI redox state in mammalian cells. *The EMBO journal* 20: 6288-6296

Molinari M, Helenius A (1999) Glycoproteins form mixed disulphides with oxidoreductases during folding in living cells. *Nature* 402: 90-93

Nguyen VD, Saaranen MJ, Karala AR, Lappi AK, Wang L, Raykhel IB, Alanen HI, Salo KE, Wang CC, Ruddock LW (2011) Two endoplasmic reticulum PDI peroxidases increase the efficiency of the use of peroxide during disulfide bond formation. *Journal of molecular biology* 406: 503-515

Nguyen VD, Wallis K, Howard MJ, Haapalainen AM, Salo KE, Saaranen MJ, Sidhu A, Wierenga RK, Freedman RB, Ruddock LW *et al* (2008) Alternative conformations of the x region of human protein disulphide-isomerase modulate exposure of the substrate binding b' domain. *Journal of molecular biology* 383: 1144-1155

Noi K, Yamamoto D, Nishikori S, Arita-Morioka K, Kato T, Ando T, Ogura T (2013) High-speed atomic force microscopic observation of ATP-dependent rotation of the AAA+ chaperone p97. *Structure (London, England : 1993)* 21: 1992-2002

Okumura M, Kadokura H, Inaba K (2015) Structures and functions of protein disulfide isomerase family members involved in proteostasis in the endoplasmic reticulum. *Free radical biology & medicine* 83: 314-322

662 Okumura M, Noi K, Kanemura S, Kinoshita M, Saio T, Inoue Y, Hikima T, Akiyama S,
663 Ogura T, Inaba K (2019) Dynamic assembly of protein disulfide isomerase in catalysis
664 of oxidative folding. *Nature chemical biology* 15: 499-509
665
666 Robinson PJ, Bulleid NJ (2020) Mechanisms of Disulfide Bond Formation in Nascent
667 Polypeptides Entering the Secretory Pathway. *Cells* 9
668
669 Robinson PJ, Kanemura S, Cao X, Bulleid NJ (2020) Protein secondary structure
670 determines the temporal relationship between folding and disulfide formation. *The*
671 *Journal of biological chemistry* 295: 2438-2448
672
673 Robinson PJ, Pringle MA, Woolhead CA, Bulleid NJ (2017) Folding of a single domain
674 protein entering the endoplasmic reticulum precedes disulfide formation. *The Journal of*
675 *biological chemistry* 292: 6978-6986
676
677 Rutkevich LA, Cohen-Doyle MF, Brockmeier U, Williams DB (2010) Functional
678 relationship between protein disulfide isomerase family members during the oxidative
679 folding of human secretory proteins. *Molecular biology of the cell* 21: 3093-3105
680
681 Rutkevich LA, Williams DB (2012) Vitamin K epoxide reductase contributes to protein
682 disulfide formation and redox homeostasis within the endoplasmic reticulum. *Molecular*
683 *biology of the cell* 23: 2017-2027
684
685 Sato Y, Inaba K (2012) Disulfide bond formation network in the three biological
686 kingdoms, bacteria, fungi and mammals. *The FEBS journal* 279: 2262-2271
687
688 Sato Y, Kojima R, Okumura M, Hagiwara M, Masui S, Maegawa K, Saiki M, Horibe T,
689 Suzuki M, Inaba K (2013) Synergistic cooperation of PDI family members in
690 peroxiredoxin 4-driven oxidative protein folding. *Scientific reports* 3: 2456
691
692 Schulman S, Wang B, Li W, Rapoport TA (2010) Vitamin K epoxide reductase prefers
693 ER membrane-anchored thioredoxin-like redox partners. *Proceedings of the National*
694 *Academy of Sciences of the United States of America* 107: 15027-15032
695
696 Sugio S, Kashima A, Mochizuki S, Noda M, Kobayashi K (1999) Crystal structure of
697 human serum albumin at 2.5 A resolution. *Protein engineering* 12: 439-446

Tavender TJ, Bulleid NJ (2010) Molecular mechanisms regulating oxidative activity of the Ero1 family in the endoplasmic reticulum. *Antioxidants & redox signaling* 13: 1177-1187

Tavender TJ, Springate JJ, Bulleid NJ (2010) Recycling of peroxiredoxin IV provides a novel pathway for disulphide formation in the endoplasmic reticulum. *The EMBO journal* 29: 4185-4197

Tian G, Xiang S, Noiva R, Lennarz WJ, Schindelin H (2006) The crystal structure of yeast protein disulfide isomerase suggests cooperativity between its active sites. *Cell* 124: 61-73

Uchihashi T, Watanabe YH, Nakazaki Y, Yamasaki T, Watanabe H, Maruno T, Ishii K, Uchiyama S, Song C, Murata K *et al* (2018) Dynamic structural states of ClpB involved in its disaggregation function. *Nature communications* 9: 2147

Wang C, Yu J, Huo L, Wang L, Feng W, Wang CC (2012) Human protein-disulfide isomerase is a redox-regulated chaperone activated by oxidation of domain a'. *The Journal of biological chemistry* 287: 1139-1149

Zhang Y, Wölfle T, Rospert S (2013) Interaction of nascent chains with the ribosomal tunnel proteins Rpl4, Rpl17, and Rpl39 of Saccharomyces cerevisiae. *The Journal of biological chemistry* 288: 33697-33707

Figure 1 - Disulfide bond introduction into RNC 69-aa and 82-aa by PDI and ERp46

A Schematic structure of plasmids constructed in this study. 'uORF2' is an arrest sequence that serves to stall translation of the upstream protein and thereby prepare stable ribosome-nascent chain complexes (RNCs). The bottom cartoon represents the location of cysteines and disulfide bonds in HSA domain I. HSA domain I consists of 195 amino acids and contains five disulfide bonds and one free cysteine at residue 34. A green box indicates the pro-sequence. Orange circles and red lines indicate cysteines and native disulfide bonds, respectively. The region predicted to be buried in the ribosome exit tunnel is shown by a cyan box.

B Domain organization of PDI and ERp46. Redox-active Trx-like domains with a CGHC motif are indicated by cyan boxes, while redox-inactive ones in PDI are by light-green boxes. Note that the PDI **b'** domain contains a substrate-binding hydrophobic pocket.

C, **E** Time course of PDI-, ERp46-, and glutathione (no enzyme)-catalyzed disulfide bond introduction into RNC 69-aa (C) and 82-aa (E). 'noSS' and '1SS' denote reduced and single-disulfide-bonded species of HSA nascent chains, respectively. Note that faint bands observed between "no SS" and "1SS" likely represent a species in which one of cysteines is not subjected to mal-PEG modification due to glutathionylation. In support of this, these minor bands are even fainter under the conditions of no GSH/GSSG.

D, **F** Quantification of disulfide-bonded species for RNC 69-aa (D) and 82-aa (F) based on the results shown in (C) and (E), respectively (n = 3).

Figure 2 - Disulfide bond introduction into RNC 82-aa Cys mutants by PDI and ERp46

A Cartoon of RNC constructs used in this study. In each construct, a cysteine (represented by a black circle) was mutated to alanine. Note that RNC 82-aa C34A retains a native cysteine pairing (i.e., Cys53 and Cys62), while RNC 82-aa C53A and C62A retain a non-native pairing.

B and **C** Time course of PDI- and ERp46-catalyzed disulfide bond introduction into RNC 82-aa C34A (top), C53A (middle), and C62A (bottom) mutants. Note that faint bands observed between "no SS" and "1SS" likely represent a species in which one of

cysteines is not subjected to mal-PEG modification due to glutathionylation. Quantification of disulfide-bonded species of RNC 82-aa Cys mutants is based on the results shown for the upper raw data (n = 3).

D Formation of a mixed disulfide bond between RNC 82-aa mono-Cys mutants and PDI (upper)/ERp46 (lower). 'Mixed' and 'No SS' denote a mixed disulfide complex between PDI/ERp46 and RNC mono-Cys mutants and isolated RNC 82-aa, respectively. Note that faint bands observed between 'Mixed' and 'no SS' are likely non-specific bands, as they were seen at the same position regardless of which 82-aa mono-Cys mutant was tested or whether an RNC was reacted with PDI or ERp46.

E Quantification of mixed disulfide species based on the results shown in (D). n = 3.

F The cartoon on the left shows possible steric collisions between ribosomes and PDI when Cys62 attacks the mixed disulfide between Cys53 on RNC 82-aa and PDI (left). The cartoon on the right shows that ERp46 can avoid this steric collision due to its higher flexibility and domain arrangement.

Figure 3 - Correlation of the distance between Cys residues and the ribosome exit site with the efficiency of disulfide bond introduction by PDI/ERp46

A Cartoons of RNC constructs with [SG]-repeat insertions. A $[SG]_5$ or $[SG]_{10}$ repeat sequence was inserted into RNC-82 aa C34A immediately after Cys62.

B, **D** PDI- (B) and ERp46 (D)-mediated disulfide bond introduction into RNC 82-aa C34A with insertion of $[SG]_5$ (upper) or $[SG]_{10}$ (lower) repeats after Cys62.

C, **E** Quantification of disulfide-bonded species (1SS) based on the results shown in (B) and (D). n = 3 for PDI and 2 for ERp46.

F Formation of a mixed disulfide bond between the 82-aa mono-Cys mutant with a $[SG]_{10}$ repeat and PDI (upper)/ERp46 (lower). Note that bands observed between 'Mixed' and 'no SS' are likely non-specific bands, as they were seen at the same position regardless of which 82-aa mono-Cys $[SG]_{10}$ mutant was tested or whether an RNC was reacted with PDI or ERp46.

G Quantification of mixed disulfide species based on the results shown in (F). n = 3.

Figure 4 - Disulfide bond introduction into RNC 95-aa by PDI and ERp46

A Schematic structure of RNC-95-aa. Orange circles and red lines in the bottom cartoon indicate cysteines and native disulfides, respectively. The region predicted to be buried in the ribosome exit tunnel is shown by a cyan box.

B Time course of PDI (0.1 μM)-, ERp46 (0.1 μM)-, and their mixture (0.1 μM each)-catalyzed disulfide bond introduction into RNC 95-aa. 'noSS' and '1SS' denote reduced and single-disulfide-bonded species of the HSA nascent chain, respectively.

C Quantification of the single-disulfide-bonded (1 SS) species based on the result shown in (B) (n = 3).

Figure 5 - High-speed AFM analysis of ERp46

A AFM images (scan area, 200 × 200 Å; scale bar, 30 Å) for ERp46 V-shape (left) and O-shape (right) conformations.

B Left upper: Histograms of circularity calculated from AFM images of ERp46. Values represent the average circularity (mean ± s.d.) calculated from curve fitting with a single- (middle and right) or two- (left) Gaussian model. Left lower: Histograms of height calculated from AFM images of ERp46. Values represent the average height (mean ± s.d.) calculated from curve fitting with a single-Gaussian model. Right: Two-dimensional scatterplots of the height versus circularity for ERp46 molecules observed by HS-AFM.

C Time-course snapshots of oxidized ERp46 captured by HS-AFM. The images were traced for 10 s. See also Movie EV1.

D Time trace of the circularity of an ERp46 molecule.

E Histogram of the circularity of ERp46 calculated from the time-course snapshots shown in (D).

Figure 6 - Single-molecule observation of PDI/ERp46 acting on 82-aa CA RNC by high-speed atomic force microscopy

A The AFM images (scan area, 500 Å × 500 Å; scale bar, 100 Å) displaying 82-aa CA RNC in the absence of PDI family enzymes on a Ni^{2+}-coated mica surface. The surface model on the right side of each AFM image illustrates ribosome whose view angle is approximately adjusted to the observed RNC particle. 40S and 60S ribosomal subunits are shown in red and blue, respectively.

B Upper AFM images (scan area, 500 Å × 500 Å; scale bar, 100 Å) displaying 82-aa CA

RNC in the presence of oxidized PDI (1 nM). PDI molecules that appear to bind 82-aa CA RNC are marked by red squares. Lower images (scan area, 250 Å × 250 Å; scale bar, 50 Å) highlight the regions surrounded by red squares in the upper images.

C Upper AFM images (scan area, 500 Å × 500 Å; scale bar, 100 Å) displaying 82-aa CA RNC in the presence of oxidized ERp46 (1 nM). ERp46 molecules that appear to bind 82-aa CA RNC are marked by blue squares. Lower images (scan area, 250 Å × 250 Å; scale bar, 50 Å) highlight the regions surrounded by blue squares in the upper images.

D Histograms of the RNC binding time of the PDI monomer (left), the PDI dimer (middle), and ERp46 (right), calculated from the observed AFM images.

E Histograms of the distance between the edge of the ribosome and the centers of RNC-neighboring PDI (left) and ERp46 (right) molecules, calculated from the observed AFM images. Values represent the average distance (mean ± s.d.) calculated from curve fitting with a single-Gaussian model.

Figure 7 - Role of the PDI hydrophobic pocket in PDI-mediated disulfide bond introduction into RNC 82-aa

A Disulfide bond introduction into RNC 82-aa by PDI I289A (upper) and ERp57 (lower). Note that faint bands observed between “no SS” and “1SS” likely represent a species in which one of cysteines is not subjected to mal-PEG modification due to glutathionylation. In support of this, these minor bands are even fainter under the conditions of no GSH/GSSG.

B Quantification of disulfide-bonded species based on the results shown in (A). Quantifications for ERp46 and PDI are based on the results shown in Fig 1E and 1F. n = 3.

C HS-AFM analyses for binding of PDI I289A to RNC CA 82-aa. Upper AFM images (scan area, 500 Å × 500 Å; scale bar, 100 Å) display the PDI I289A molecules that bind 82-aa CA RNC, as marked by red squares. Lower images (scan area, 250 Å × 250 Å; scale bar, 50 Å) highlight the regions surrounded by red squares in the upper images.

D Histograms show the distribution of the RNC binding time of the PDI I289A monomers (left) and dimers (right).

852 **E** Histogram shows the distribution of the distance between the edge of the ribosome
853 and the centers of RNC-neighboring PDI I289A molecules, calculated from the
854 observed AFM images. Values represents the average distance (mean ± s.d.) calculated
855 from curve fitting with a single-Gaussian model.
856
857 **Figure 8 - Proposed model of co-translational disulfide bond introduction into**
858 **nascent chains by ERp46 and PDI**
859 During the early stages of translation, ERp46 introduces disulfide bonds through
860 transient binding to a nascent chain. For efficient disulfide introduction by ERp46, a
861 pair of cysteines must be exposed by at least ~8 amino acids from the ribosome exit site.
862 By contrast, PDI introduces disulfide bonds by holding a nascent chain inside the
863 central cavity of the PDI homodimer during the later stages of translation, where a pair
864 of cysteines must be exposed by at least ~18 amino acids from the ribosome exit site.
865 However, when a longer polypeptide is exposed outside the ribosome, ERp46- or
866 PDI-mediated disulfide bond formation can be slower, possibly due to formation of
867 higher-order conformation in the nascent chain. Longer nascent chains may allow PDI
868 family enzymes to compete with each other for binding and acting on RNC.

Table 1 – Primers used in this study

No.	plasmid name	template	mutation position	primer name	nucleic acid sequence (5'-3')
1	82 aa C34A	82 aa	C34A	HSA C34A FW	cag tat ctt cag cag gcc cca ttt gaa gat cat
				HSA C34A RV	atg atc ttc aaa tgg ggc ctg ctg aag ata ctg
2	82 aa C53A	82 aa	C53A	HSA C53A FW	gaa ttt gca aaa aca gcc gtt gct gat gag tca
				HSA C53A RV	tga ctc atc agc aac ggc tgt ttt tgc aaa ttc
3	82 aa C62A	82 aa	C62A	HSA C62A FW	gag tca gct gaa aat gcc gac aaa tca ctt cat
				HSA C62A RV	atg aag tga ttt gtc ggc att ttc agc tga ctc
4	82 aa mono-Cys34	82 aa C53A	C62A	HSA C62A FW	gag tca gct gaa aat gcc gac aaa tca ctt cat
				HSA C62A RV	atg aag tga ttt gtc ggc att ttc agc tga ctc
5	82 aa mono-Cys53	82 aa C34A	C62A	HSA C62A FW	gag tca gct gaa aat gcc gac aaa tca ctt cat
				HSA C62A RV	atg aag tga ttt gtc ggc att ttc agc tga ctc
6	82 aa mono-Cys62	82 aa C34A	C53A	HSA C53A FW	gaa ttt gca aaa aca gcc gtt gct gat gag tca
				HSA C53A RV	tga ctc atc agc aac ggc tgt ttt tgc aaa ttc
7	82 aa C34A $[SG]_5$	82 aa C34A	between L74 and C75	C34A 5rpt 10rpt FW2	ggc agc ggc agc ggc tgc aca gaa ttc atg cag
				C34A SG5rpt RV	gcc gct gcc gct gcc gct gcc gct gcc gct taa ttt gtc tcc aaa aag
8	82 aa C34A $[SG]_{10}$	82 aa C34A	between L74 and C75	C34A 5rpt 10rpt FW2	ggc agc ggc agc ggc tgc aca gaa ttc atg cag
				C34A SG10rpt RV	gcc gct gcc gct gcc gct gcc gct gcc gct gcc gct gcc gct gcc gct gcc gct taa ttt gtc tcc aaa aag

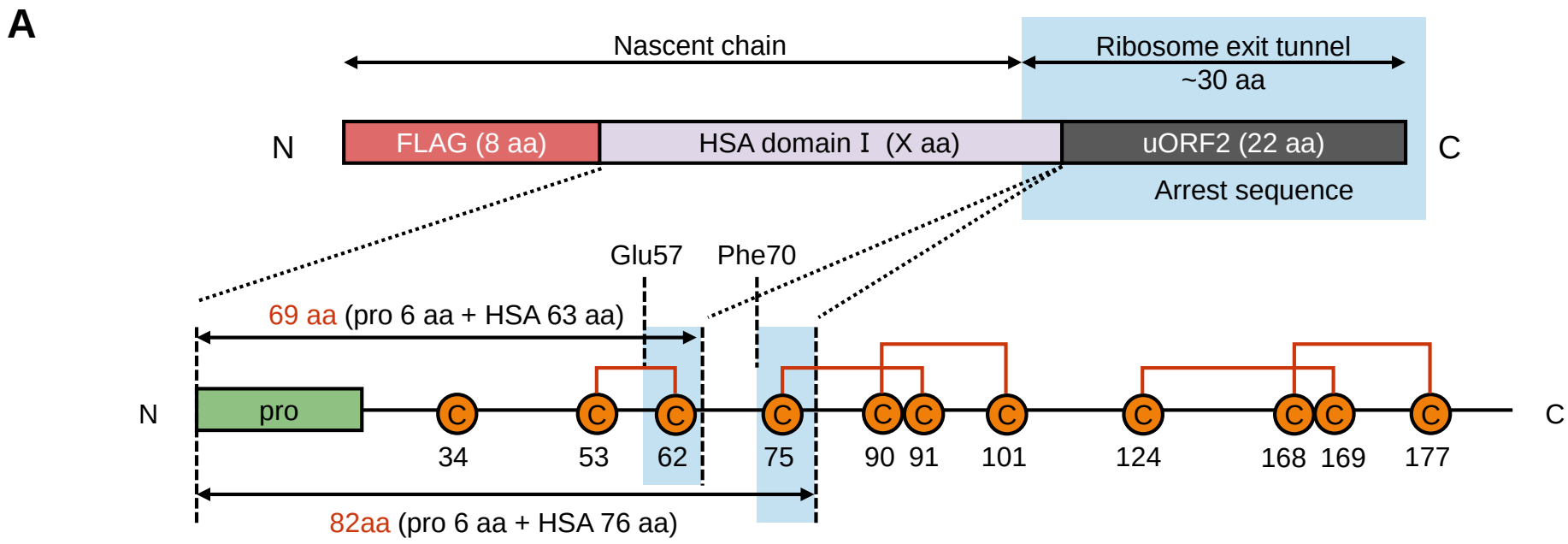

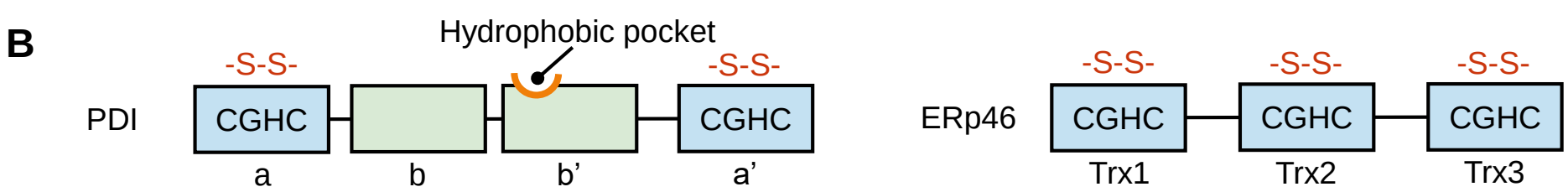

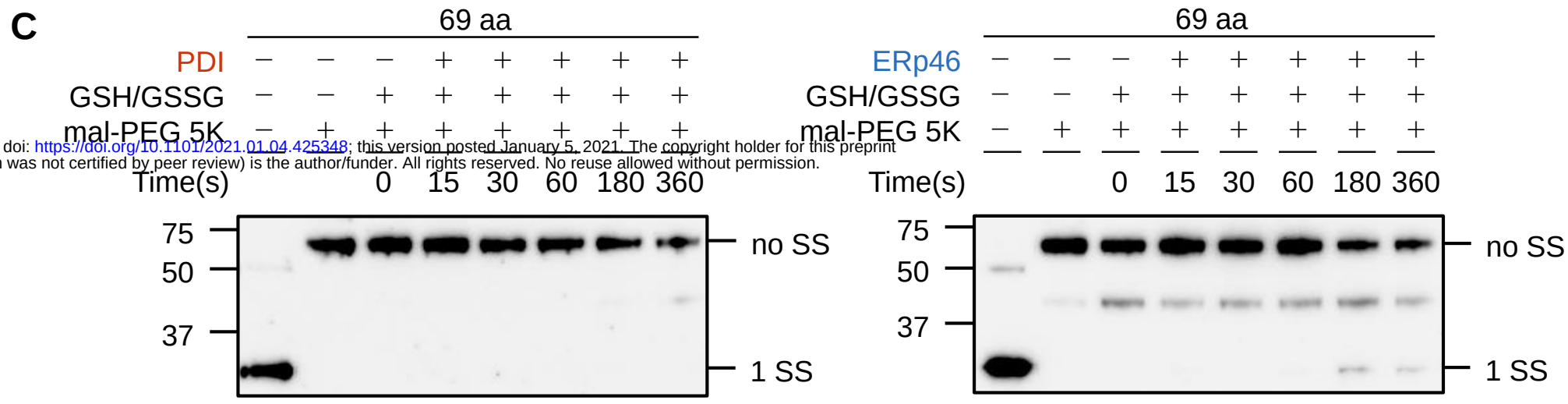

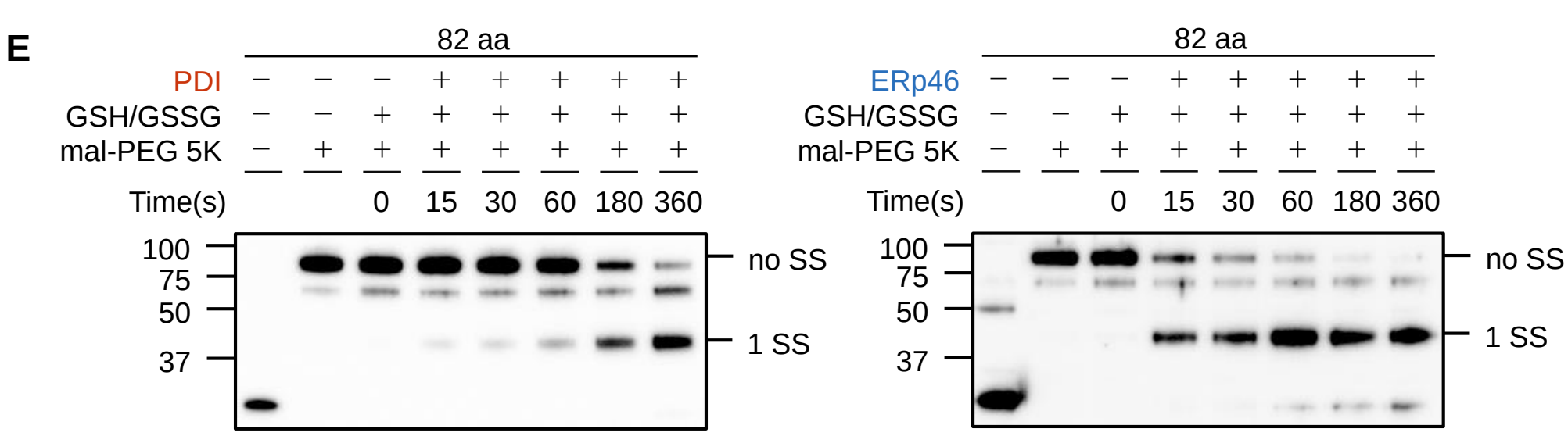

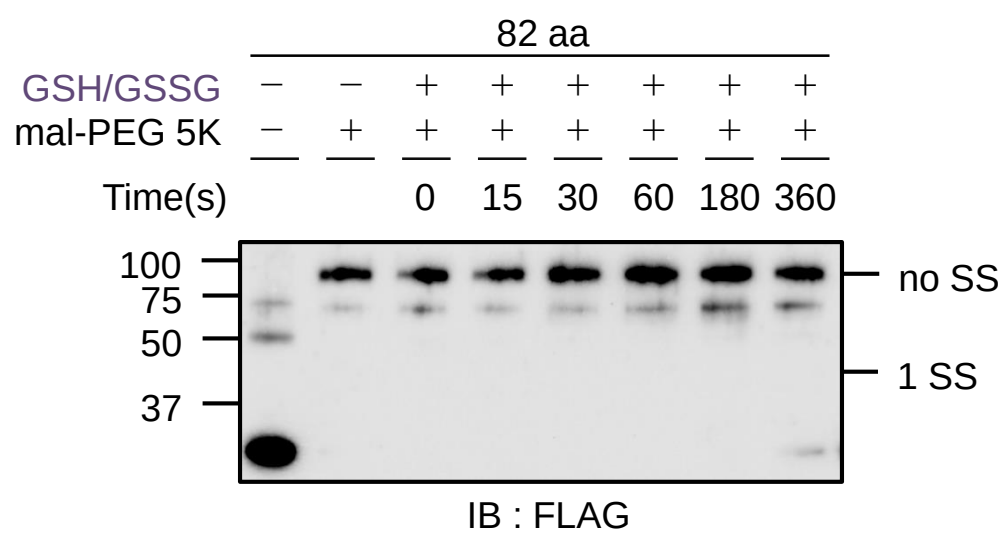

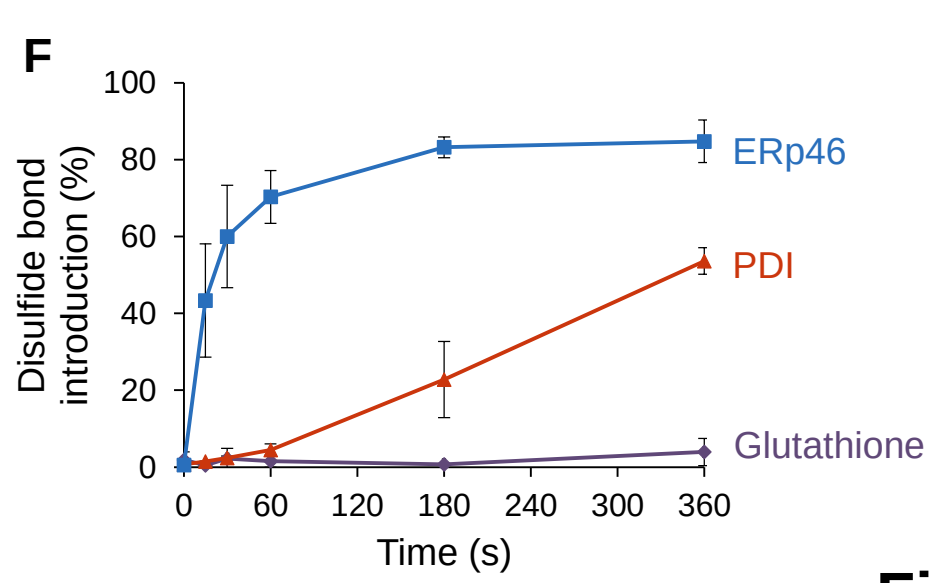

Fig.1

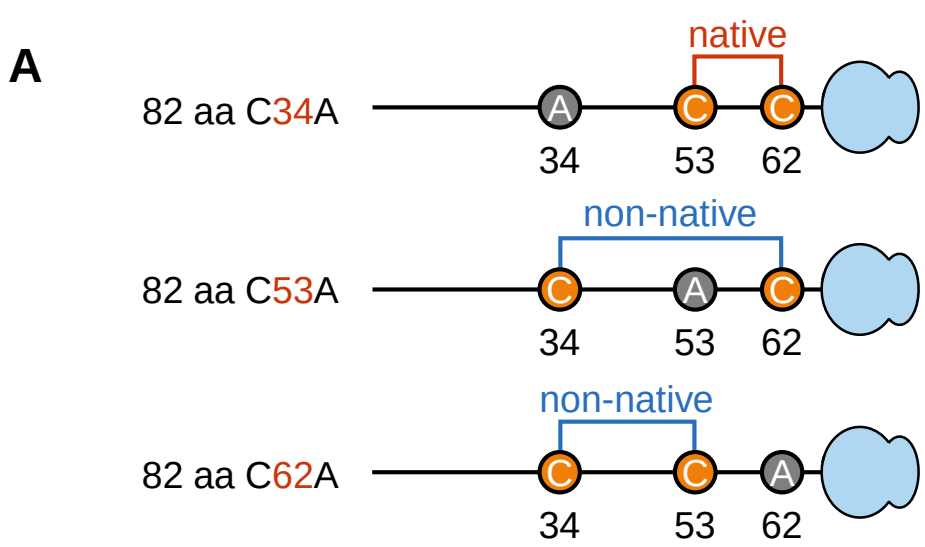

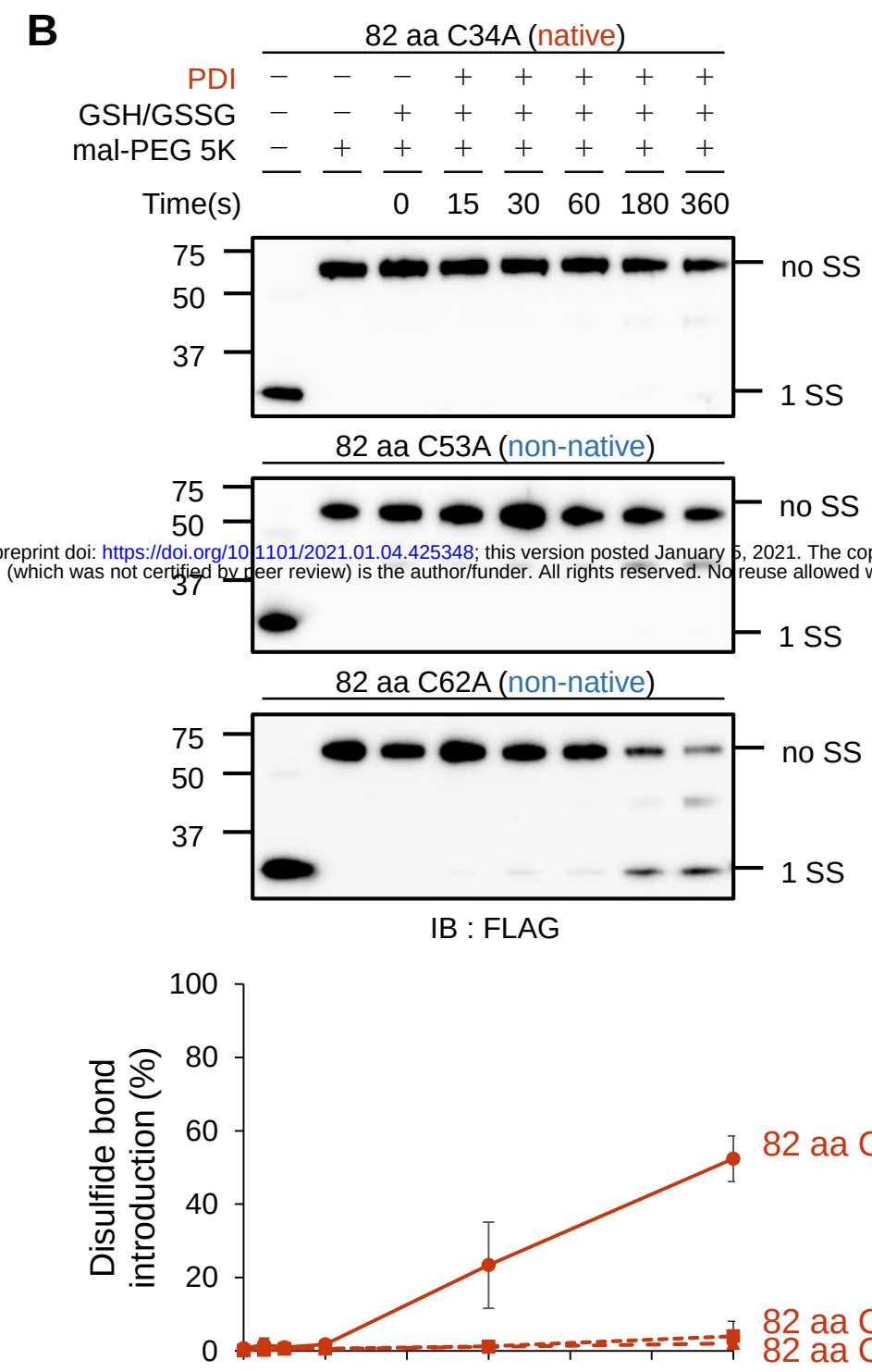

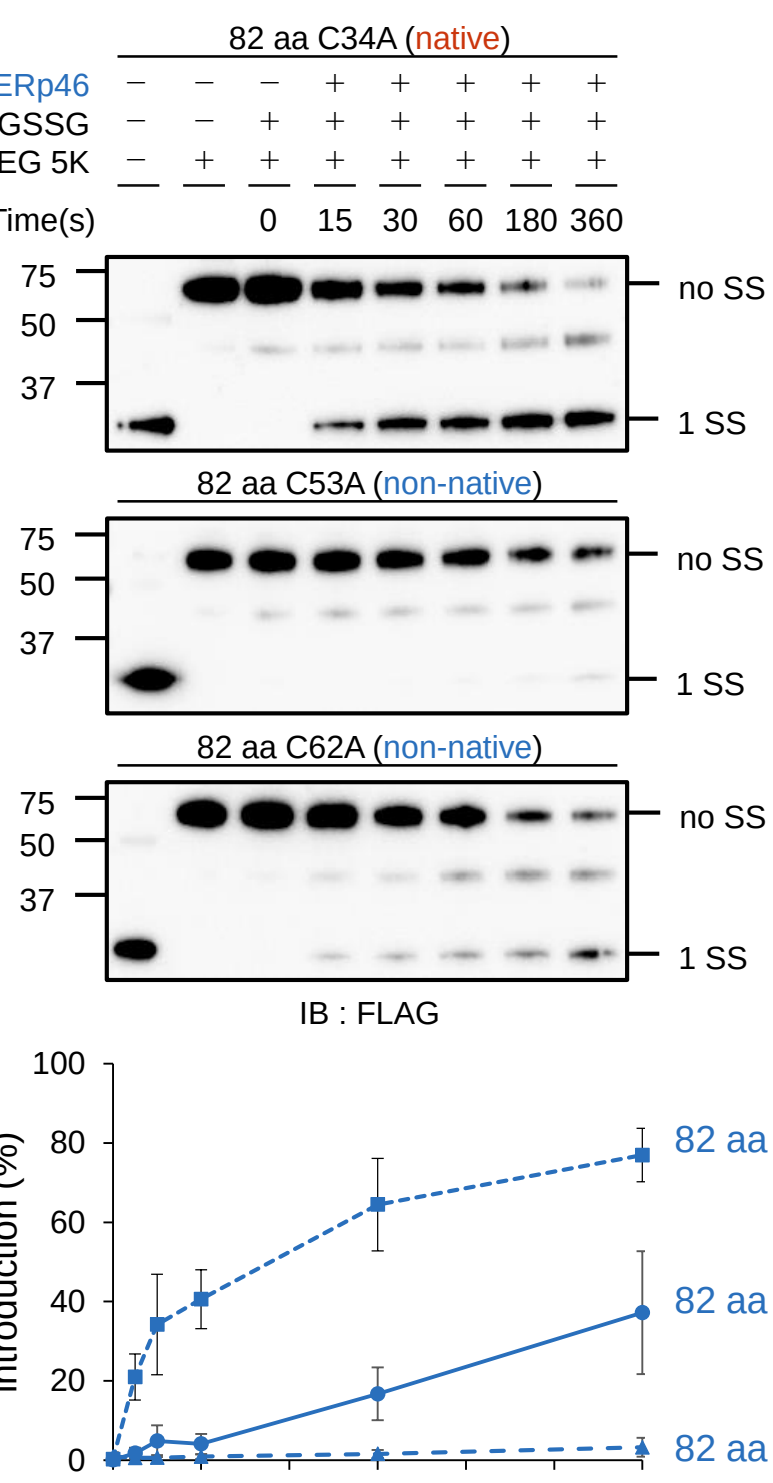

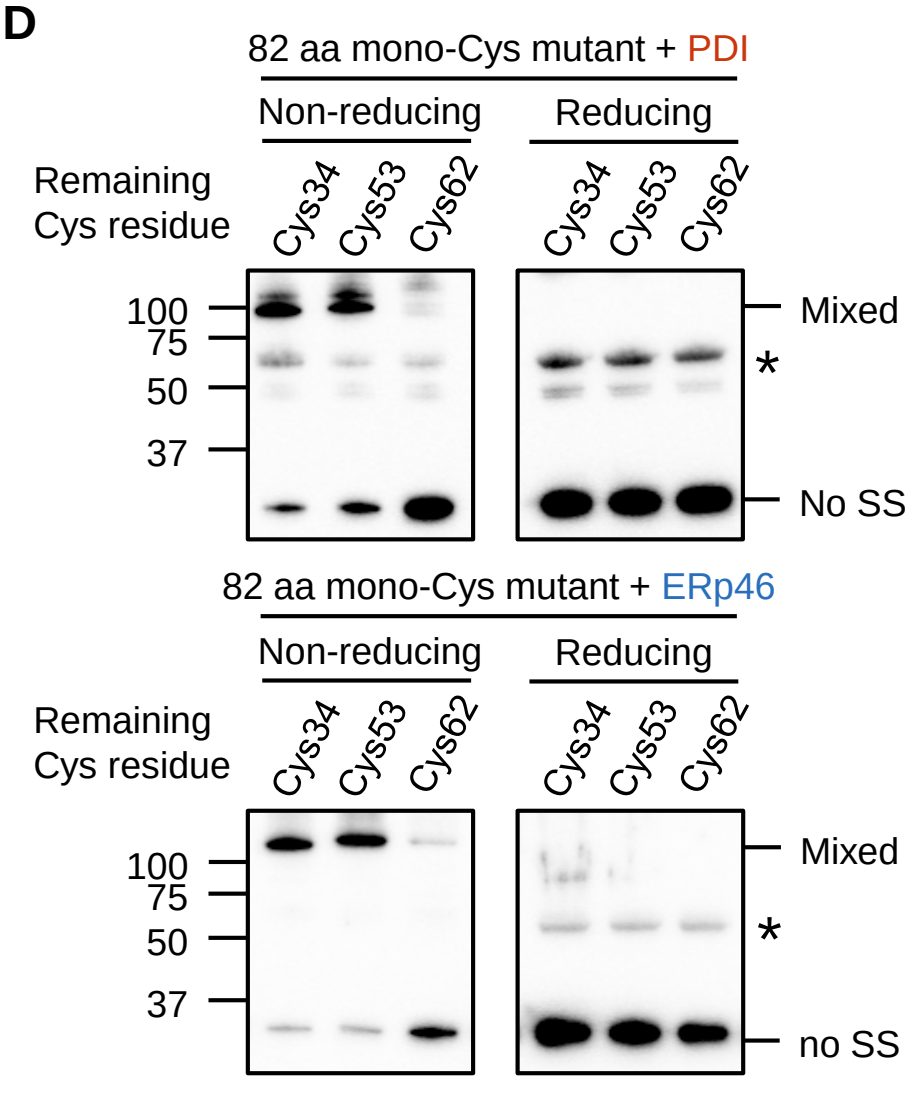

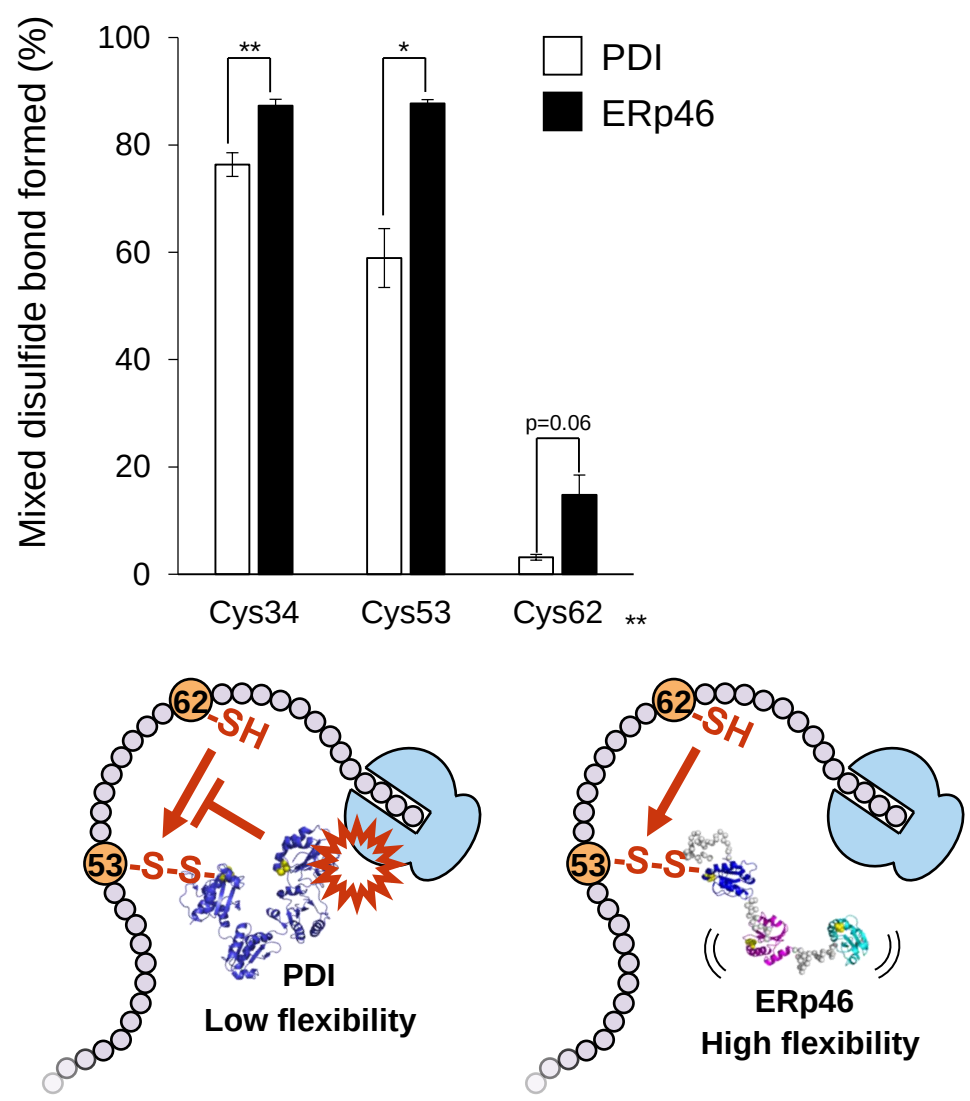

Fig.2

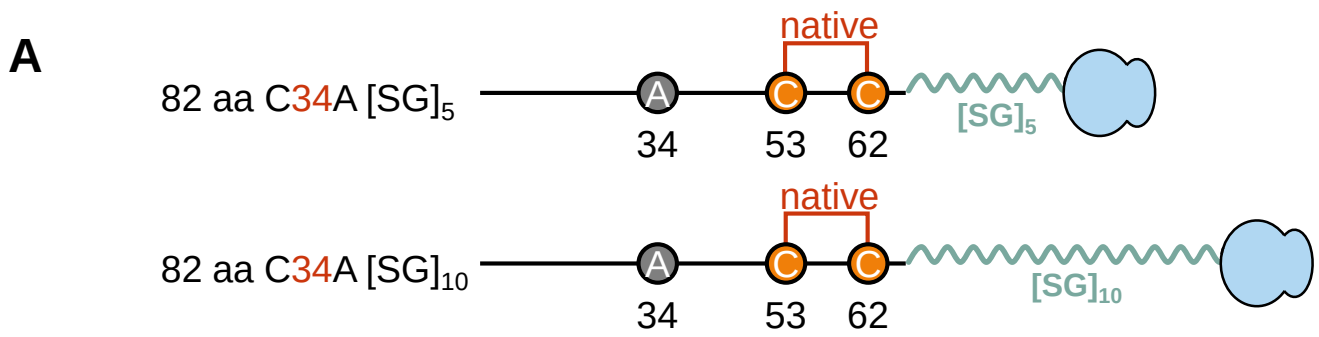

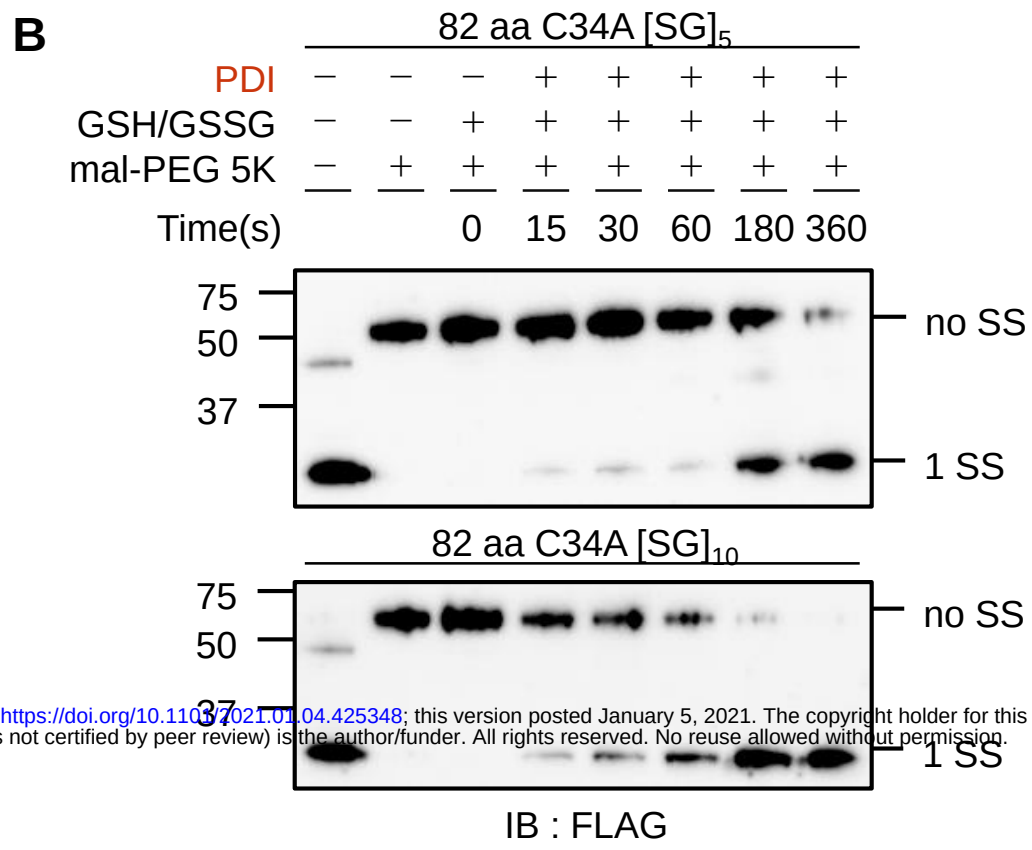

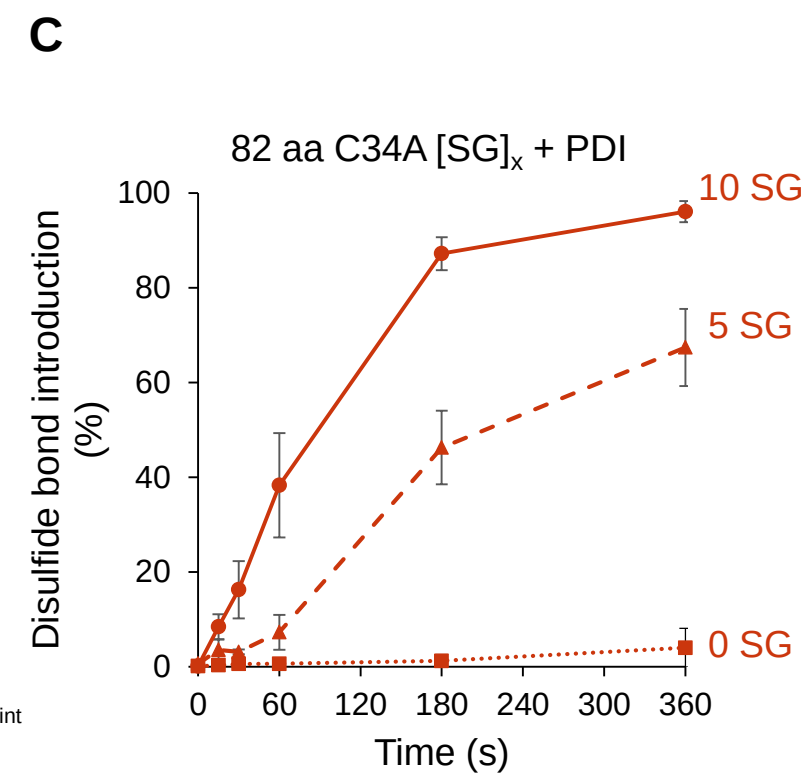

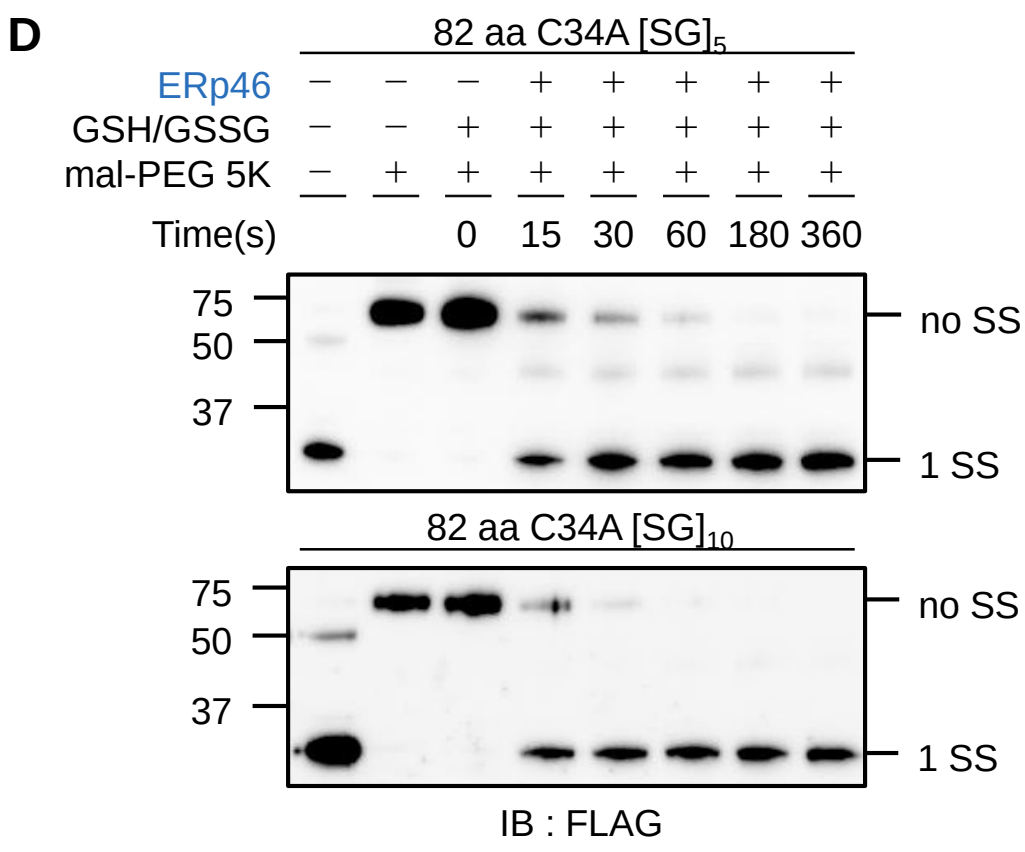

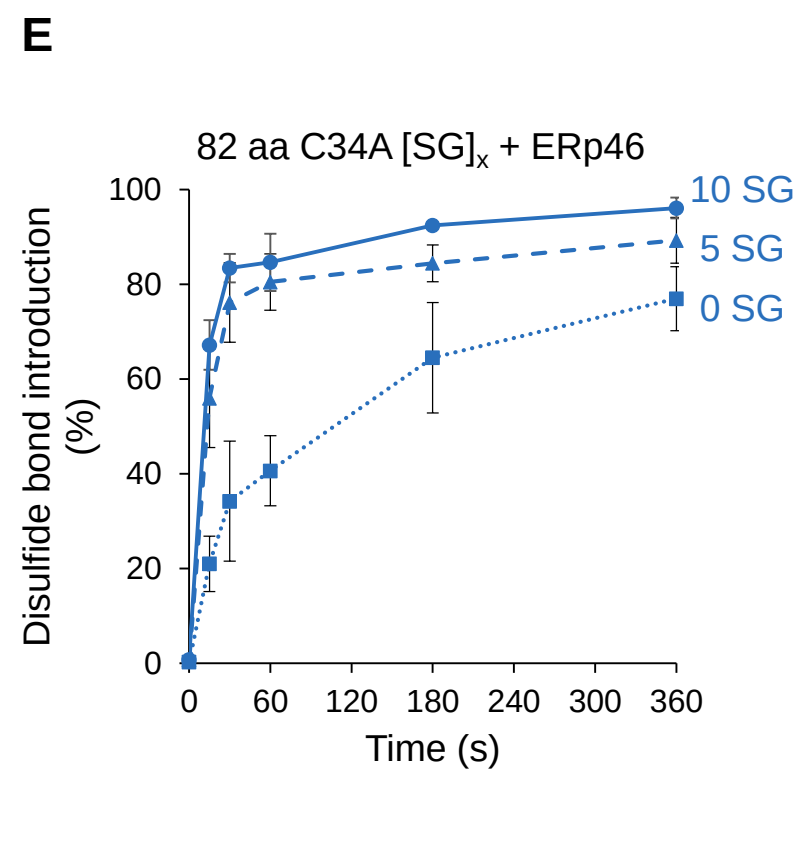

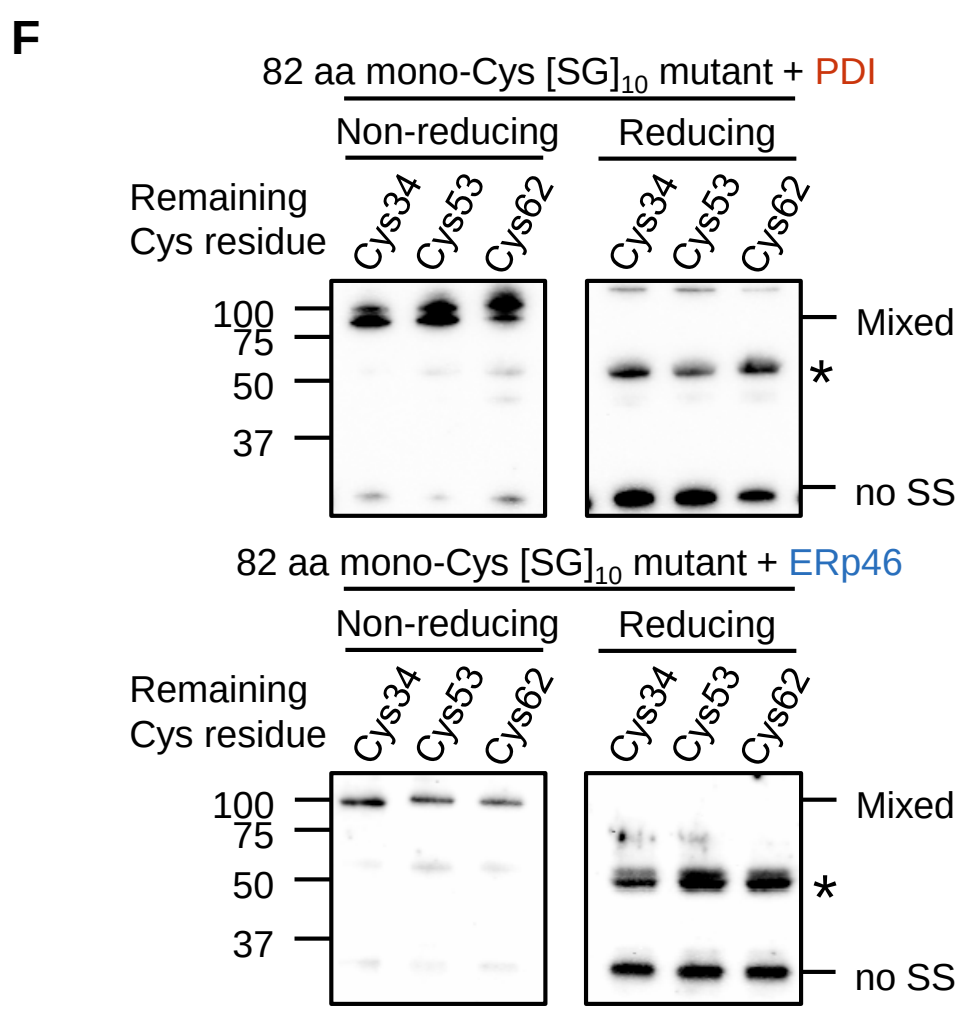

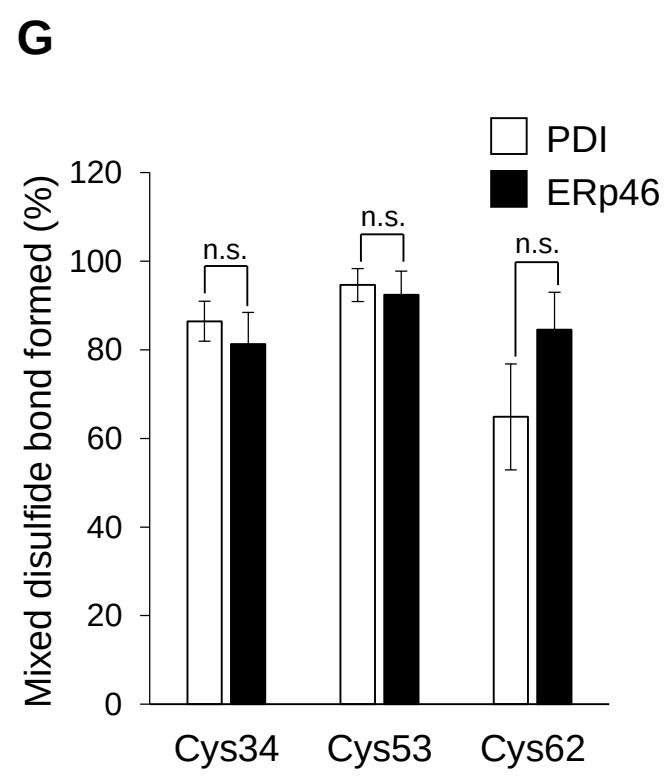

Fig.3

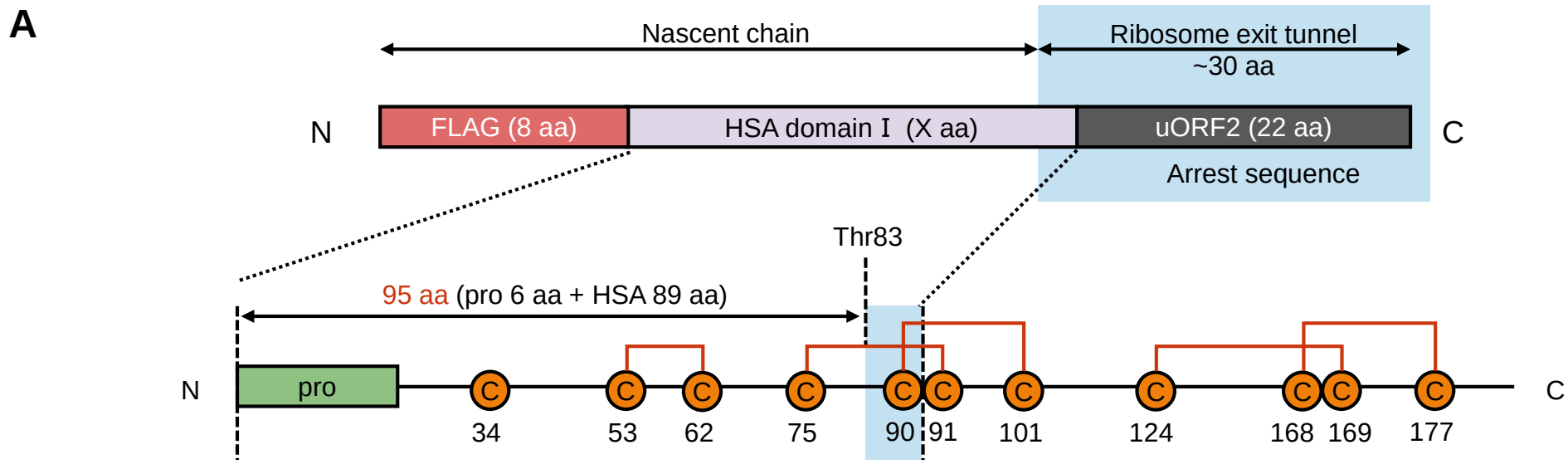

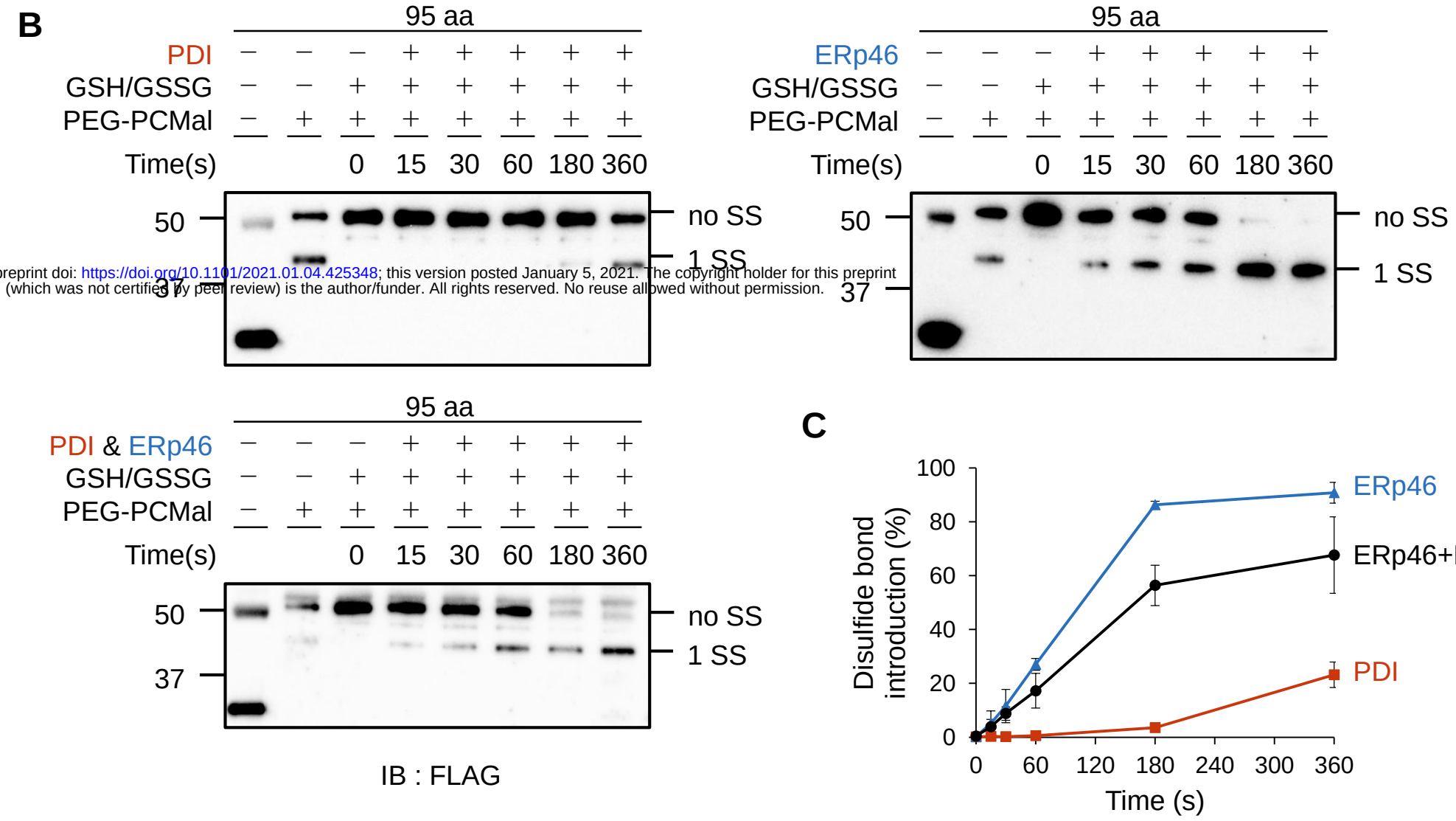

IB : FLAG

Fig.4

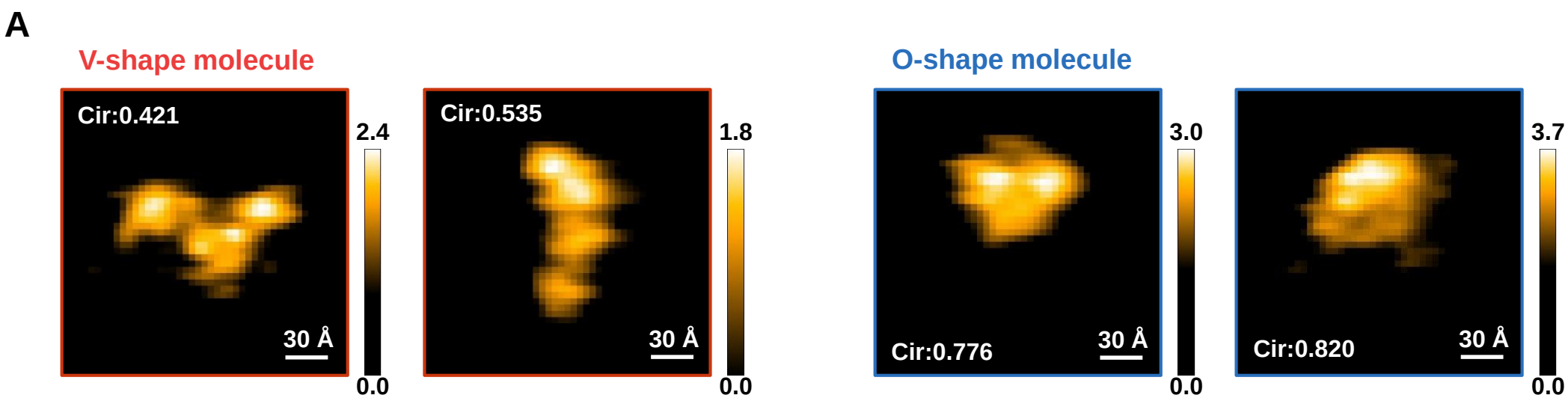

Fig.5

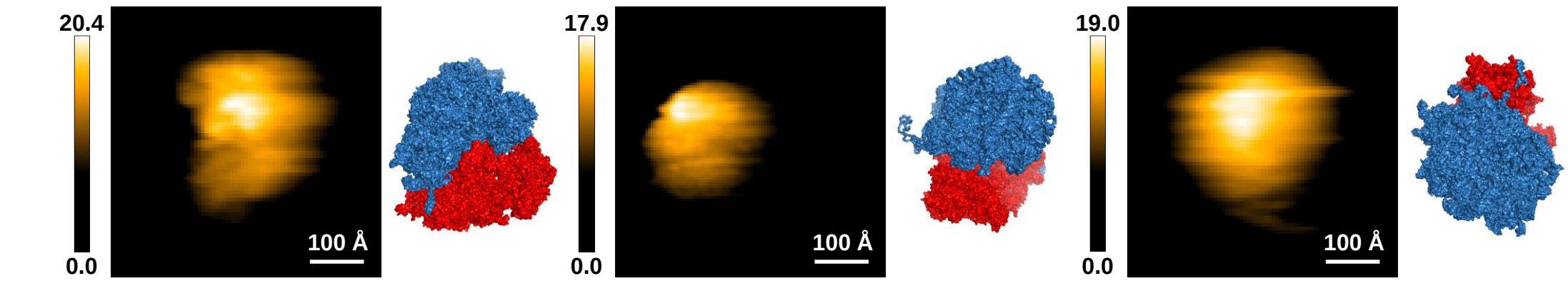

Fig. 6

A

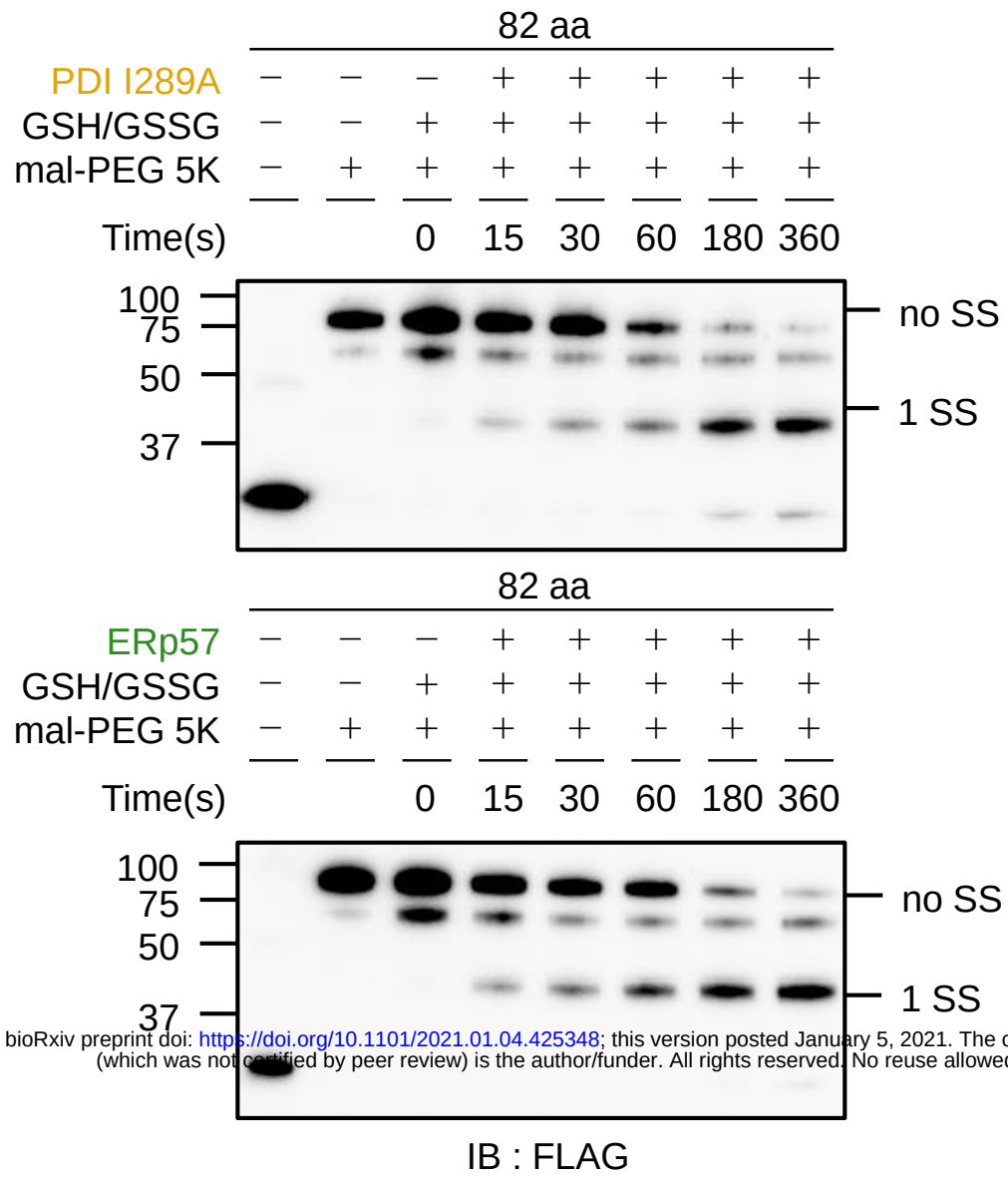

B

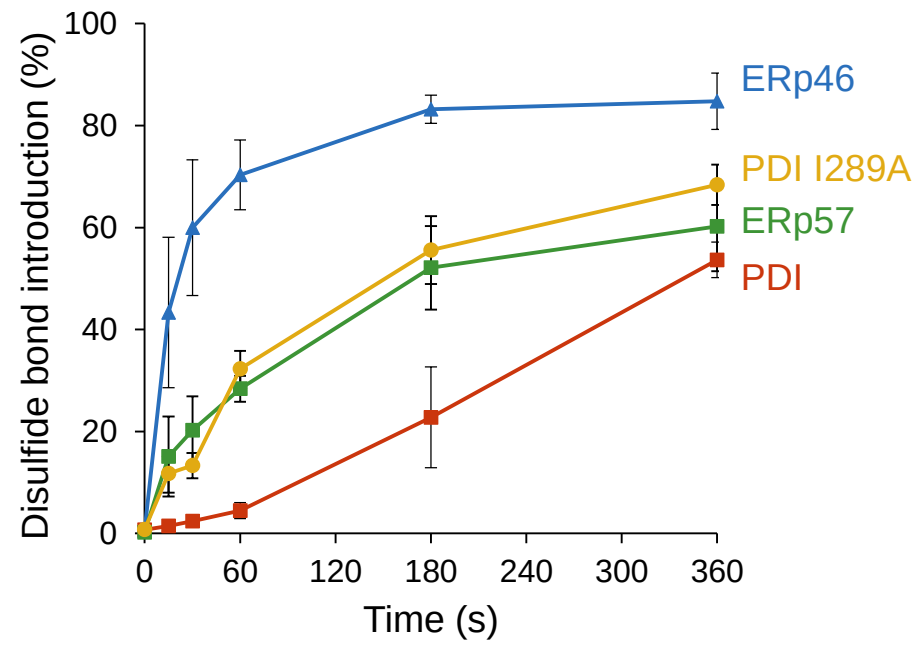

C

82-aa CA RNC + Oxidized PDI I289A

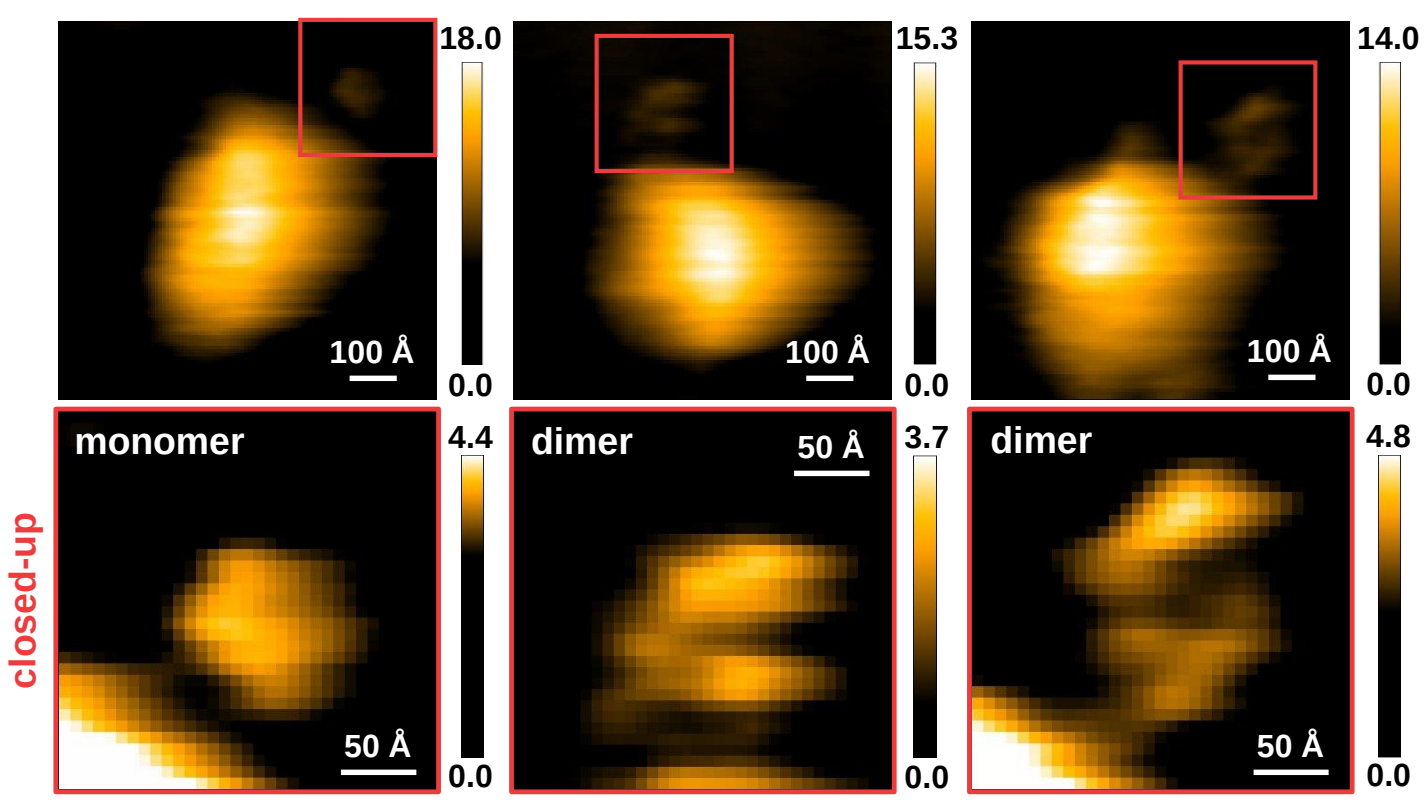

D

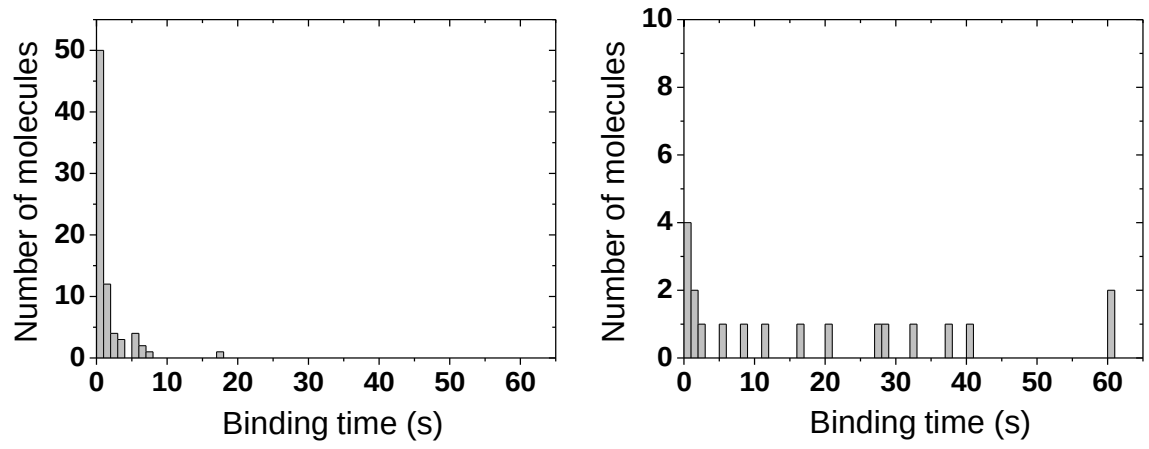

E

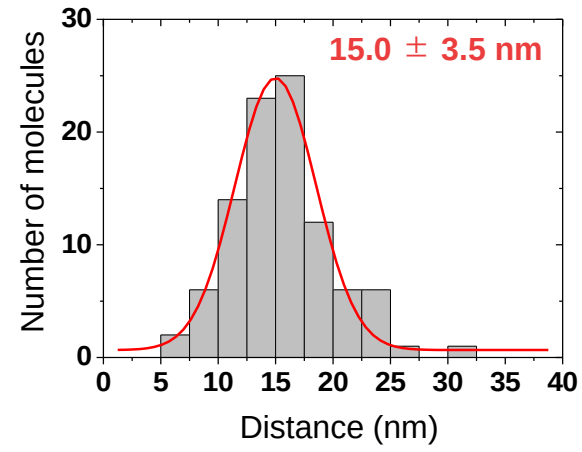

Fig. 7

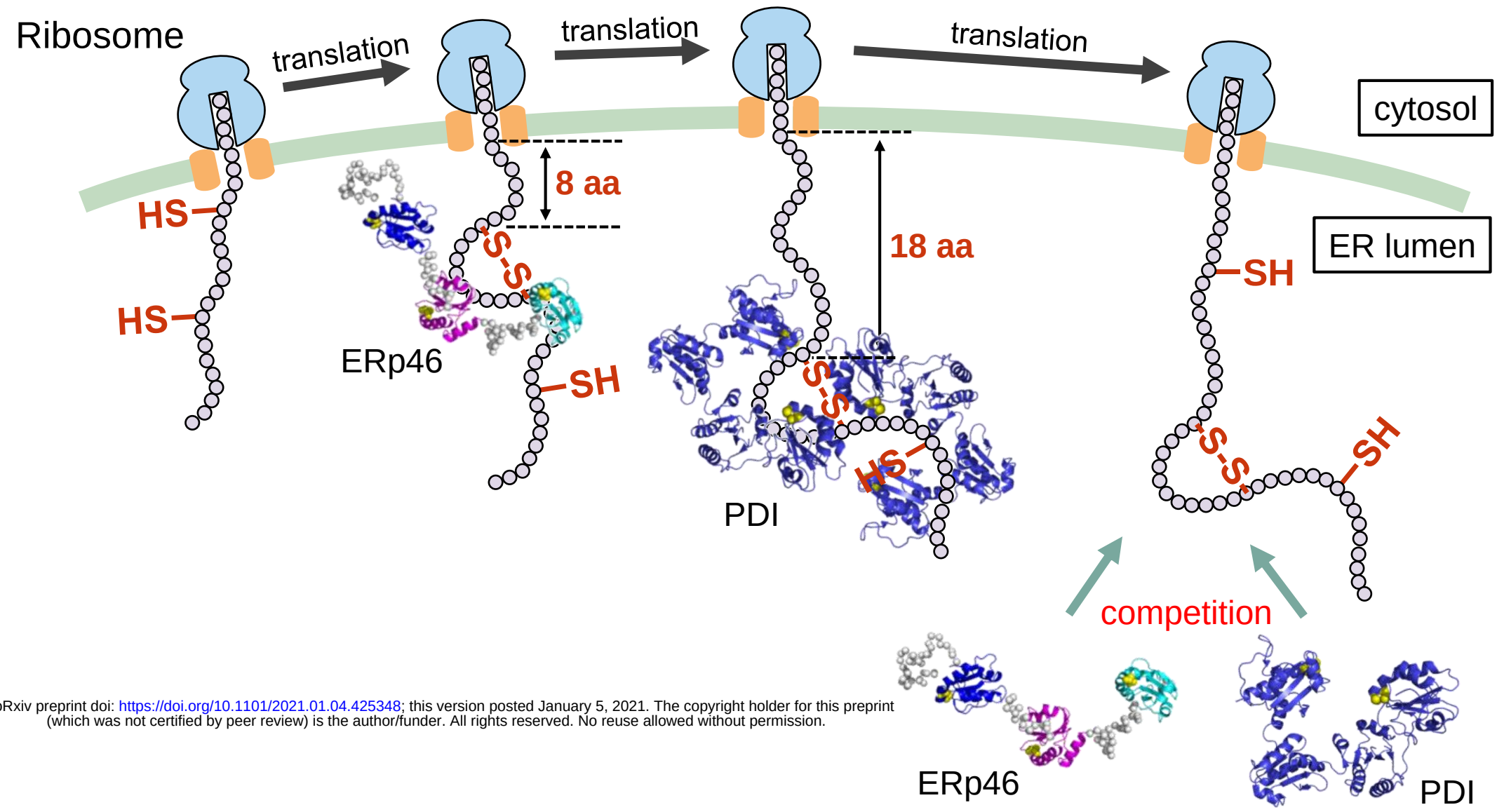

Fig. 8

1 **Expanded View**

2

3 **Distinct roles and actions of PDI family enzymes in catalysis of nascent-chain**
4 **disulfide formation**

5

6 Chihiro Hirayama[1], Kodai Machida[2#], Kentaro Noi[3#], Tadayoshi Murakawa[4], Masaki
7 Okumura[1,5], Teru Ogura[6,7], Hiroaki Imataka[2], and Kenji Inaba[1*]

8

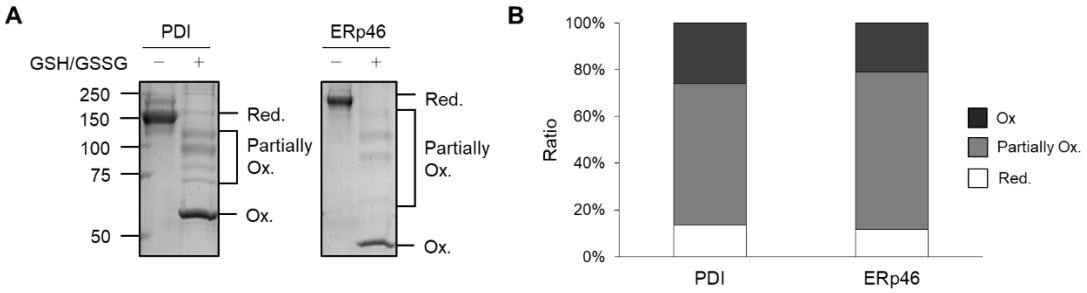

Figure EV1 - Redox states of PDI and ERp46 in glutathione redox buffer and disulfide bond introduction into 82 aa C34A, catalyzed by PDI a domain

A Redox states of PDI and ERp46 in the presence of 1 mM GSH and 0.2 mM GSSG. Purified PDI and ERp46 were incubated for 6 mins at 30 ºC in the above glutathione redox buffer and modified with 2 mM mal-PEG 5K for separation on SDS gels.

B Quantification based on the results shown in (A).

19

A

	RNC only	RNC bound to PDI/ERp46	RNC bound to many PDI/ERp46 molecules	total
NC-RNC	94	11	0	105
NC-RNC + PDI	106	15	0	121
NC-RNC + PDI I289A	87	16	0	103
NC-RNC + ERp46	81	16	3	100
82-aa CA RNC	116	10	0	126
82-aa RNC CA + PDI	141	69	11	221
82-aa RNC CA + PDI I289A	115	73	15	203
82-aa RNC CA + ERp46	117	59	25	201

B

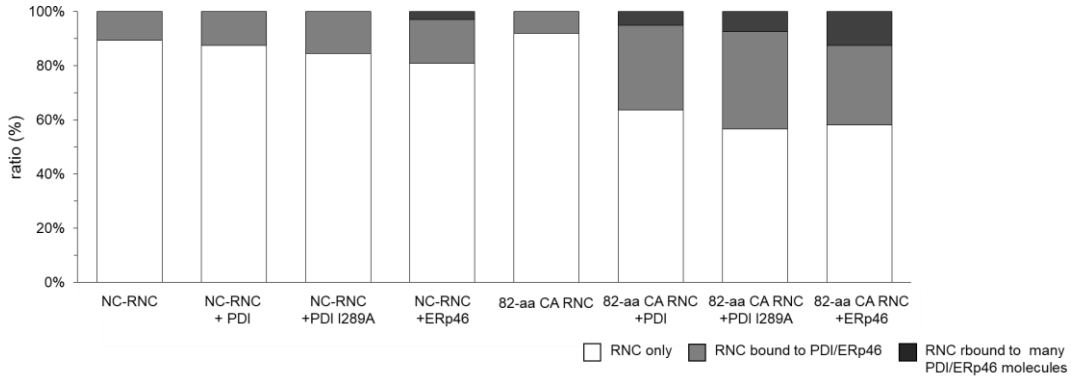

20

21 **Figure EV2 - Statistical analysis of RNC molecules observed by HS-AFM in the**
22 **presence or absence of PDI/ERp46**

23 **A** Number of particles observed for NC-RNC or 82-aa CA RNC molecules present in
24 isolation or bound to PDI/ERp46 molecules.

25 **B** Ratio of NC-RNC or 82-aa CA RNC molecules present in isolation or bound to
26 PDI/ERp46, calculated based on the observed number of particles in (A). Note that a
27 minor portion of NC-RNC or 82-aa CA RNC molecules were bound to many ERp46/PDI
28 molecules, possibly due to serious structural damages of the RNC molecules.

29

30

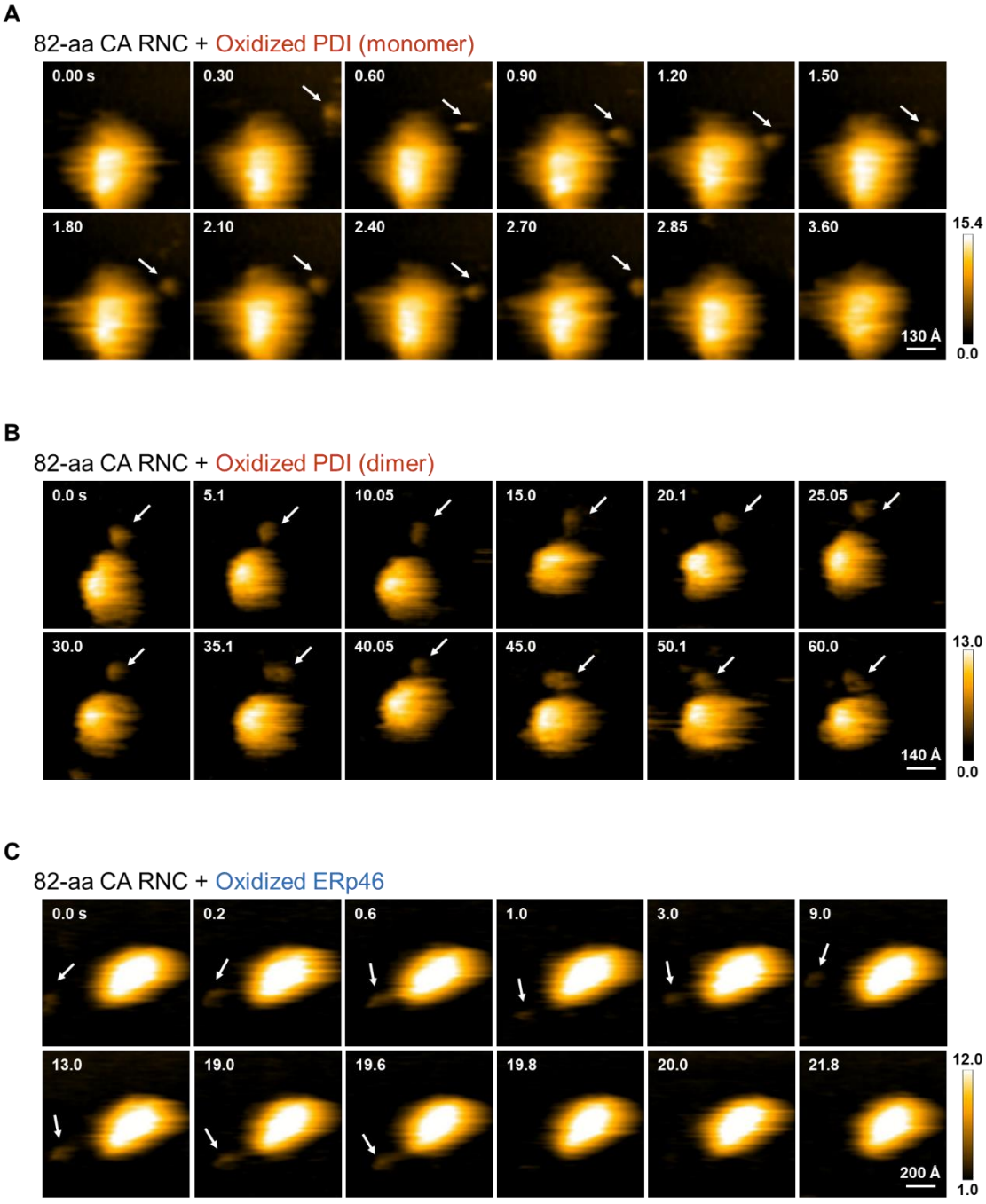

Figure EV3 - Representative time-course snapshots captured by HS-AFM for 82-aa CA RNC bound to the PDI monomer (A), the PDI dimer (B), and ERp46 (C).

A Time-course snapshots captured by HS-AFM for the PDI monomer binding to 82-aa CA RNC. The AFM images (scan area, 650 Å × 650 Å; scale bar, 130 Å) displaying 82-aa CA RNC in the presence of oxidized PDI (1 μM). White arrows indicate the monomeric PDI molecules that bind to 82-aa CA RNC. See also supplementary video 2.

B Time-course snapshots captured by HS-AFM for the PDI dimer binding to 82-aa CA RNC. The AFM images (scan area, 700 Å × 700 Å; scale bar, 140 Å) displaying 82-aa CA RNC in the presence of oxidized PDI (1 μM). White arrows indicate the dimeric PDI molecules that bind to 82-aa CA RNC. See also supplementary video 3.

C Time-course snapshots captured by HS-AFM for ERp46 binding to 82-aa CA RNC. The AFM images (scan area, 1,000 Å × 1,000 Å; scale bar, 200 Å) displaying 82-aa CA RNC in the presence of oxidized ERp46 (1 μM). White arrows indicate the ERp46 molecules that bind to 82-aa CA RNC. See also supplementary video 4.

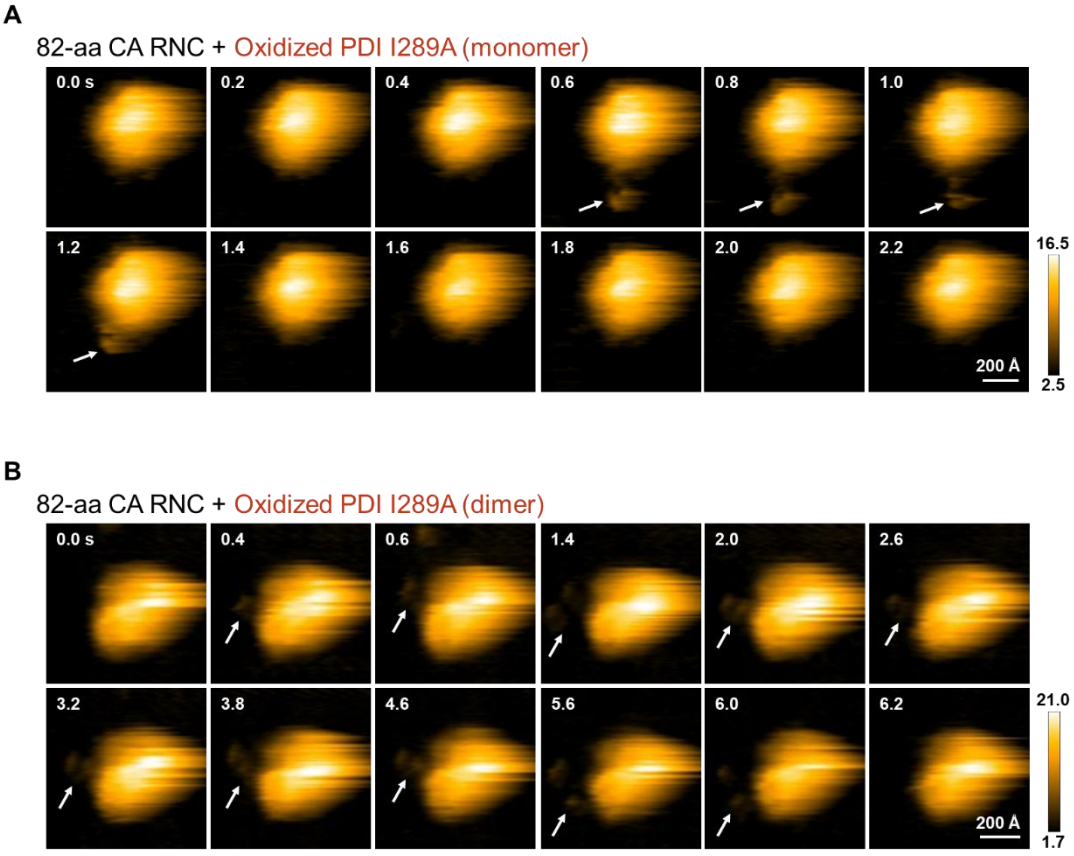

Figure EV4 - Representative time-course snapshots captured by HS-AFM for 82-aa CA RNC bound to the PDI I289A monomer (A), and the PDI I289A dimer (B).

A Time-course snapshots captured by HS-AFM for the PDI I289A monomer binding to 82-aa CA RNC. The AFM images (scan area, 900 Å × 900 Å; scale bar, 200 Å) displaying 82-aa CA RNC in the presence of oxidized PDI I289A (1 µM). White arrows indicate the monomeric PDI I289A molecules that bind to 82-aa CA RNC. See also supplementary video 5.

B Time-course snapshots captured by HS-AFM for the PDI I289A dimer binding to 82-aa CA RNC. The AFM images (scan area, 800 Å × 800 Å; scale bar, 200 Å) displaying 82-aa CA RNC in the presence of oxidized PDI I289A (1 µM). White arrows indicate the dimeric PDI I289A molecules that bind to 82-aa CA RNC. See also supplementary video 6.

Movie EV1 - HS-AFM movies showing structure dynamics of oxidized ERp46. This movie is a source of the time-course snapshots shown in Fig 5C.

Movie EV2 - HS-AFM movies showing the binding of the PDI monomer to 82-aa CA RNC. This movie is a source of the time-course snapshots shown in supplementary Fig EV3A.

Movie EV3 - HS-AFM movies showing the binding of the PDI dimer to 82-aa CA RNC. This movie is a source of the time-course snapshots shown in supplementary Fig EV3B.

Movie EV4 - HS-AFM movies showing the binding of ERp46 to 82-aa CA RNC. This movie is a source of the time-course snapshots shown in supplementary Fig EV3C.

Movie EV5 - HS-AFM movies showing the binding of the PDI I289A monomer to 82-aa CA RNC. This movie is a source of the time-course snapshots shown in supplementary Fig EV4A.

Movie EV6 - HS-AFM movies showing the binding of the PDI I289A dimer to 82-aa CA RNC. This movie is a source of the time-course snapshots shown in supplementary Fig EV4B.